Human Molecular Genetics, 2009, Vol. 18, No. 5 ***872–887***
doi:10.1093/hmg/ddn417
Advance Access published on December 12, 2008

Phosphorylation does not prompt, nor prevent, the formation of α-synuclein toxic species in a rat model of Parkinson's disease

Samareh Azeredo da Silveira[1], Bernard L. Schneider[1], Carmen Cifuentes-Diaz[3,†], Daniel Sage[2,†], Toufik Abbas-Terki[1], Takeshi Iwatsubo[4], Michaël Unser[3] and Patrick Aebischer[1,*]

[1]Brain Mind Institute and [2]Biomedical Imaging Group, Ecole Polytechnique Fédérale de Lausanne (EPFL), CH-1015 Lausanne, Switzerland, [3]INSERM, U839, Institut du Fer à Moulin, 75005 Paris, France and [4]Department of Neuropathology and Neuroscience, Graduate School of Pharmaceutical Sciences, University of Tokyo, Tokyo 113-0033, Japan

Received September 23, 2008; Revised and Accepted December 7, 2008

Phosphorylation is involved in numerous neurodegenerative diseases. In particular, alpha-synuclein is extensively phosphorylated in aggregates in patients suffering from synucleinopathies. However, the share of this modification in the events that lead to the conversion of alpha-synuclein to aggregated toxic species needed to be clarified. The rat model that we developed through rAAV2/6-mediated expression of alpha-synuclein demonstrates a correlation between neurodegeneration and formation of small filamentous alpha-synuclein aggregates. A mutation preventing phosphorylation (S129A) significantly increases alpha-synuclein toxicity and leads to enhanced formation of beta-sheet-rich, proteinase K-resistant aggregates, increased affinity for intracellular membranes, a disarrayed network of neurofilaments and enhanced alpha-synuclein nuclear localization. The expression of a mutation mimicking phosphorylation (S129D) does not lead to dopaminergic cell loss. Nevertheless, fewer but larger aggregates are formed, and signals of apoptosis are also activated in rats expressing the phosphorylation-mimicking form of alpha-synuclein. These observations strongly suggest that phosphorylation does not play an active role in the accumulation of cytotoxic pre-inclusion aggregates. Unexpectedly, the study also demonstrates that constitutive expression of phosphorylation-mimicking forms of alpha-synuclein does not protect from neurodegeneration. The role of phosphorylation at Serine 129 in the early phase of Parkinson's disease is examined, which brings new perspective to therapeutic approaches focusing on the modulation of kinases/phosphatases activity to control alpha-synuclein toxicity.

INTRODUCTION

Phosphorylation–dephosphorylation is involved in the regulation of nearly all processes of life. About one-third of mammalian proteins are covalently bound to phosphate. The conformational change in the structure of the protein induced by the binding of a phosphate is responsible for the activation or deactivation of enzymes and receptors. Phosphorylation also plays a role in interaction with protein partners and, in some cases, functions as a signal for degradation. Phosphorylation is involved in a number of neurodegenerative diseases. In particular, phosphorylated alpha-synuclein (α-syn) was shown to be present in aggregates in patients suffering from dementia with Lewy bodies, from multiple system atrophy, from brain iron accumulation type I and from Parkinson's disease (PD) (1–5). Alpha-syn has generated much interest for its role in PD. It is persistently found to be the major component of the hallmark neuronal inclusions named Lewy bodies (6–10), and genetic mutations of α-syn have been linked to familial forms of parkinsonism and associated with idiopathic PD (6,8,10–15). Serine at position 129 (Ser129) has been identified as the major phosphate acceptor site of α-syn in PD cases (1,3,5,16–18).

*To whom correspondence should be addressed. Tel: +41 216939505; Fax: +41 216939520; Email: patrick.aebischer@epfl.ch
†These authors contributed equally to this work.

The occurrence of phosphorylation raises the question of its share in the events that lead to the conversion of α-syn to toxic species, particularly in sporadic PD. An ascendant interpretation is that transient protofibrils are the cytotoxic species, whereas inclusion bodies are the result of a neuronal protective strategy channeling misfolded toxic load and converting it into an inert body (19–26). In the present study, single amino acid mutants of α-syn have been used to address this question. Ser129 is converted either to an alanine (S129A) with the aim of abolishing phosphorylation or to a negatively charged residue, aspartate (S129D), with the aim of mimicking some of the effects of phosphorylation (27). Although the adequacy of aspartate as a substitute to reproduce the effects of phosphorylation is still discussed and the impact of other characteristics of the phosphate group, such as its steric hindrance (28) or conformational changes (29), are still being investigated, the S129D mutant is being widely used. The impact of these modifications on the cytotoxic properties of the protein, on the one hand, and on its aggregation, on the other hand, are being examined. Conflicting results have been obtained *in vitro* and also *in vivo* between transgenic *Drosophila* (30) and recombinant adeno-associated vector (rAAV)-injected rats expressing these Ser129 variants (31). S129A enhanced the formation of inclusions and spared *Drosophila* from neurodegeneration, but markedly increased neuronal cell loss in the substantia nigra (SN) of rats. Likewise, S129D enhanced toxicity in *Drosophila*, whereas dopaminergic neuronal loss was virtually absent in S129D-injected rats. These divergences have raised the question of the adequacy of the fly as a model for PD, in view of its nervous system and its lack of any endogenous homolog to α-syn (32,33).

The present study was undertaken to further understand the cellular and morphological changes responsible for the observed discrepancies between non-phosphorylated and phosphorylated α-syn. For this purpose, we based our experimental design on the unilateral stereotaxic injection of rAAV vectors into the SN of rats. Recombinant pseudotyped rAAV2/6 vectors were engineered to express wild-type (WT) human α-syn as well as human α-syn with either the S129A or S129D mutation. In order to assess the impact of the A30P familial mutation, human A30P α-syn and its S129A and S129D variants were engineered. We provide evidence that the enhanced loss of dopaminergic neurons, already caused at a low level of expression of the S129A variants, correlates with increased deposition of small filamentous α-syn aggregates, increased association of α-syn with intracellular membranes and neurofilaments and increased nuclear localization. Our results indicate that phosphorylation does not play a role in the formation of pre-Lewy body toxic α-syn species. Nonetheless, we also show that phosphorylation does not protect from neurodegeneration, as evidenced by the formation of aggregates and the activation of markers of apoptosis following the expression of the phosphorylation-mimicking S129D variants.

RESULTS

Opposed impacts of S129A and S129D on dopaminergic neuron survival already at a low level of expression

To investigate the pathogenic potency of recombinant pseudotyped rAAV2/6-mediated expression of Ser129-mutated α-syn, we performed unilateral stereotaxic injections of six vectors, respectively, into one hemisphere of the SN. The rAAV2/6 vector variants expressed the following forms of α-syn: human WT protein, human α-syn bearing the A30P familial mutation and WT or A30P α-syn submitted to site-directed mutagenesis converting their serine at position 129 either to alanine (S129A) or to aspartate (S129D). Infection of 293T cells showed that all constructs yielded comparable levels of expression (Fig. 1A). The use of an antibody specifically recognizing α-syn phosphorylated at Ser129 (PSer129 antibody) (1) revealed the increased accumulation of monomeric and oligomeric forms of α-syn, following transduction with viral particles coding for intact Ser129 α-syn when compared with α-syn S129A and α-syn S129D (Fig. 1B). Western blot analyses disclosed mild non-specific binding of the antibody, but quantification and normalization to tubulin substantiated the distinctly increased intensity of the monomeric and oligomeric bands in WT α-syn cell extracts. This was then confirmed *in vivo*. PSer129 staining was indeed positive in the SN of rats injected with intact Ser129 α-syn, whereas no staining was observed in rats injected with α-syn S129A or α-syn S129D (Fig. 1C). Infectivity was also evaluated *in vivo*, 8 weeks after unilateral injection. AAV vectors pseudotyped with a serotype 6 capsid were chosen for their high tropism for nigral dopaminergic neurons, as revealed by their extensive colocalization with tyrosine hydroxylase (TH)-positive neurons (Fig. 1D).

Injection of three increasing doses of rAAV2/6 vectors coding for WT α-syn yielded a dose-dependent loss, from 11 to 22%, in the number of neurons positive for the dopaminergic-specific TH marker in the injected SN (Fig. 1E). We used the same rationale of increasing doses in our phosphorylation analysis. The S129A mutation dramatically increased the pathology, whereas S129D was less neurotoxic, even when the viral preparation was not diluted. The increase in α-syn S129A toxicity was dose-dependent, reaching a loss of over 70% of TH-positive neurons in rats injected with non-diluted viral particles. The α-syn WT form displayed stronger toxicity than the A30P mutant. This difference was however not statistically significant, and the divergent patterns of toxicity between intact Ser129, S129A and S129D were the same in the case of the α-syn WT and A30P backbones. The loss of dopaminergic neurons was confirmed by results obtained with VMAT2 (vesicular monoamine transporter 2) (data not shown). Finally, the optical density (OD) of dopaminergic fibers projecting to the striatum decreased by ∼16% in S129A brains following the injection of 1.4×10^7 transduction units (TUs) and displayed differences between the S129 variants similar to those obtained in the SN (Fig. 1F).

In order to measure the level of expression at which these events occurred, injected and non-injected SN of three animals per group were extracted and homogenized. The total levels of expression of the vectors, when compared with the level of endogenous α-syn in the non-injected SN, were evaluated by western blot analyses, with the use of an antibody recognizing both human and rat α-syn (Fig. 1G). Quantitative comparison allowed to roughly estimate that the mean total level of expression of α-syn was double that of the rat endogenous protein alone.

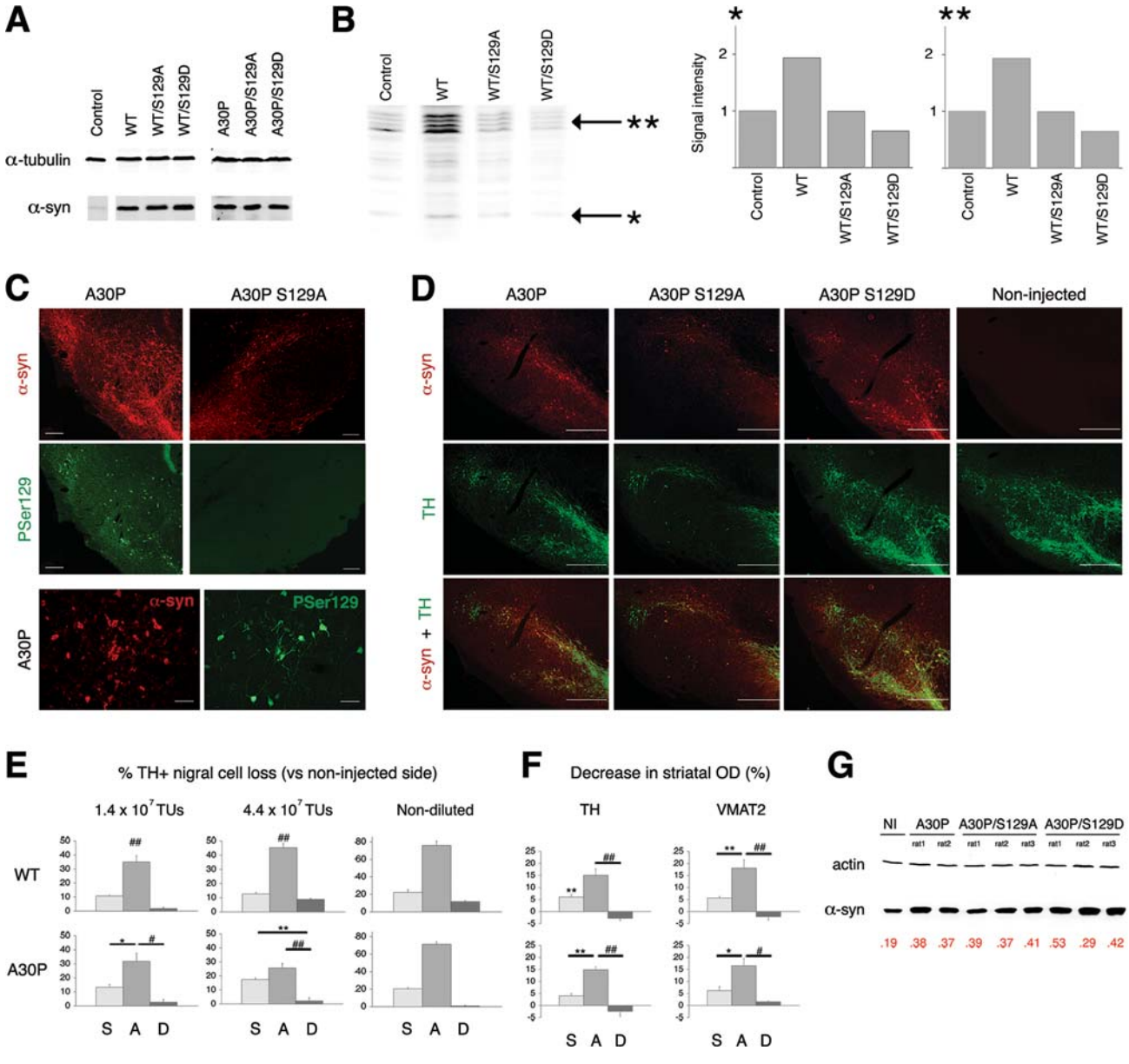

Figure 1. S129A mutation markedly enhances α-syn toxicity, whereas it is hindered by S129D mutation, in rats expressing the transgene at a level comparable to that of the endogenous protein. (**A**) Expression of α-syn variants in infected 293T cells when compared with non-infected cells. (**B**) Fifty micrograms of proteins from non-infected 293T cells and cells infected with either AAV-CMV-α-syn-WT, AAV-CMV-α-syn-WT/S129A or AAV-CMV-α-syn-WT/S129D. The membrane was probed with the PSer129 antibody, which revealed the presence of monomeric (a single 16 kDa band) and oligomeric (four bands between 30 and 40 kDa) forms in cells expressing WT α-syn, when compared with the non-infected S129A and S129D samples. Histograms represent signal intensities, which were assessed by The Odyssey® Infrared Imaging System detection and normalized to tubulin. (**C**) Immunostaining showing phosphorylated α-syn in the SN of rats injected with AAV-CMV-α-syn-A30P and the absence of phosphorylation in rats injected with AAV-CMV-α-syn-A30P/S129A. Magnification in pictures at the bottom. Scale bars, four pictures on top: 200 μm and two pictures at the bottom: 50 μm. (**D**) Immunostaining showing neuronal co-expression of α-syn and TH in the SN of rats 8 weeks post-virus injection. Scale bars: 500 μm. (**E**) Significant dose-dependent loss of TH-positive neurons following the injection of 1.4×10^7 TUs, 4.4×10^7 Us and non-diluted viral suspensions. Histograms represent the loss of nigral neurons when compared with the contralateral non-injected hemisphere. The lesion created by the S129A (A) form was significantly more pronounced than that created by the native Ser129 (S) and S129D forms (D), in the case of both the wild-type backbone (WT) and the A30P backbone (A30P). One-way analysis of variance (103), followed by Scheffé's *post hoc* test, revealed a main group effect in all cases. Wild-type backbone: 1.4×10^7 TUs (S129 $n = 9$, S129A $n = 8$, S129D $n = 9$) and 4.4×10^7 TUs (S129 $n = 9$, S129A $n = 9$, S129D $n = 8$). A30P backbone: 1.4×10^7 TUs (S129 $n = 4$, S129A $n = 5$, S129D $n = 7$) and 4.4×10^7 TUs (S129 $n = 6$, S129A $n = 5$, S129D $n = 6$). As viral titers were not normalized in the experiments with non-diluted vectors, statistical analyses were not performed. $^{*}P < 0.05$, $^{**}P < 0.005$, $^{\#}P < 0.0005$, $^{\#\#}P < 0.0001$ relative to the two other groups, unless indicated otherwise. Data expressed as average ± SEM. (**F**) Comparable results were obtained with TH- and VMAT2-immunoreactivity in the striatal terminals, already at a viral dose of 1.4×10^7 TUs. $^{*}P < 0.05$, $^{**}P < 0.005$, $^{\#}P < 0.0005$, $^{\#\#}P < 0.0001$ relative to the two other groups, unless otherwise indicated. Data were expressed as average ± SEM. (**G**) Fifty micrograms of total protein from the SN of rats unilaterally injected with either AAV-CMV-α-syn-A30P, AAV-CMV-α-syn-A30P/S129A or AAV-CMV-α-syn-A30P/S129D. Numbers in red indicate the values of intensity of the α-syn-positive bands normalized to actin, as assessed by The Odyssey® Infrared Imaging System Detection. The membrane was probed with a sheep anti-α-syn antibody (AB5334P), which allowed comparison of human α-syn levels of expression with those of the rat endogenous α-syn. NI, non-injected SN.

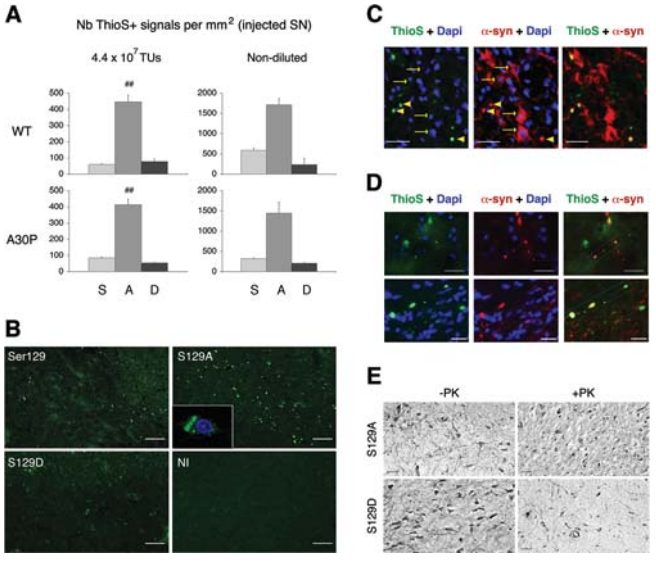

Figure 2. ThioS-positive and PK-resistant α-syn species are markedly enhanced by S129A mutation when compared with S129D mutation. (**A**) Significant dose-dependent increase in ThioS-positive signals following the injection of 4.4×10^7 TUs and non-diluted viral suspensions. Histograms represent the number of ThioS-positive aggregates per mm^2. One-way analysis of variance (103), followed by Scheffé's *post hoc* test, revealed a main group effect in all cases. As viral titers were not normalized in the experiments with non-diluted vectors, statistical analyses were not performed. WT backbone 4.4×10^7 TUs: [S129 (S) $n = 9$, S129A (A) $n = 9$, S129D (D) $n = 7$]. WT backbone non-diluted: (S129 $n = 4$, S129A $n = 6$, S129D $n = 5$). A30P backbone 4.4×10^7 TUs: (S129 $n = 6$, S129A $n = 6$, S129D $n = 6$). A30P backbone non-diluted: (S129 $n = 45$, S129A $n = 6$, S129D $n = 4$). $^{\#\#}P < 0.0001$ relative to the two other groups. Data were expressed as average ± SEM. (**B**) Immunostaining showing ThioS signal (green) in WT-, S129A- and S129D-injected rats, 8 weeks post-virus injection, when compared with the non-injected (NI) hemisphere. Scale bars, 50 μm. Inset: magnification of a neuron revealing positive ThioS signals (green) and the nucleus (Dapi staining, blue). (**C**) Immunostaining for ThioS (green) and human α-syn (red) and Dapi staining of the nuclei (blue). α-syn immunoreactivity is punctate in cells displaying ThioS-positive signals (arrowheads), when compared with cells without ThioS signals (arrows). Scale bars, 20 μm. (**D**) Colocalization of ThioS (green) and human α-syn (red) within beaded formations in neuritic processes. Scale bars, upper panels: 20 μm and lower panels: 10 μm. (**E**) Staining against human α-syn preceded by PK treatment (+PK) or not (−PK) of adjacent 25 μm slices of S129A- or S129D-injected brains. S129D-expressing SN submitted to the identical PK treatment were substantially poorer in PK-resistant α-syn. Scale bars, 50 μm.

Tight correlation between dopaminergic neuronal loss and formation of small, α-synuclein-positive, β-sheet-rich, proteinase K-resistant aggregates

The above results prompted us to examine the relation between the divergent nigral toxicities of S129A and S129D, on the one hand, and protein aggregation in the SN, on the other hand. The formation of amyloid protein aggregates was evaluated by staining with thioflavin S (ThioS) (Fig. 2A and B). Upon binding to β-pleated sheet structures, this dye undergoes a shift of its excitation spectrum, resulting in a fluorescence signal at 482 nm (34). With an injected dose of 4.4×10^7 TUs, the number of ThioS-positive signals was about six times higher in the S129A-injected brains than in the brains injected with intact Ser129 α-syn or with α-syn S129D (Fig. 2A). Moreover, although the number of these structures rose in all six groups following the injection of non-diluted viral preparations, similar differences between intact Ser129, S129A and S129D persisted. Again, for each of the Ser129 variants, numbers pertaining to WT, respectively, A30P, were markedly close.

ThioS-positive staining was restricted to the SN, and ThioS application followed by immunostaining with the use of an antibody specifically targeting human α-syn showed that the β-pleated sheet structures correspond to the human α-syn-positive pattern of expression (Fig. 2C and D). A closer examination revealed that in cells presenting ThioS signal, the pattern of expression of the transgene was less diffuse in general and highly concentrated at the ThioS-positive spots (Fig. 2C). Alpha-syn and ThioS co-staining was also positive in neuronal fibers in the SN (Fig. 2D). These fibers exhibited the colocalization most prominently in beaded formations along the fibers. Again, aggregates along neuronal processes were more abundant in the S129A-injected SN than in the SN injected with the two other forms.

Staining against human α-syn performed subsequently to proteinase K (PK) treatment of the brain slices showed a similar divergence between the Serine-mutant variants (Fig. 2E). Following digestion of PK-sensitive forms, distinct dots as well as cells with irregular cytoplasmic staining were highlighted. S129D-expressing SN submitted to the identical PK treatment were substantially poorer in PK-resistant α-syn, when compared with S129A-expressing SN. This was in agreement with the ThioS-counting results, indicating the significantly lower amount of β-pleated sheet-rich structures in the S129D groups.

Immuno-electron microscopy (IEM) analyses of the SN pars compacta of rats allowed to uphold our results obtained with ThioS signals counting and PK treatment, on the one hand, and enabled a comparative morphological analysis of nigral neurons from the six different groups of rats, on the other hand. IEM analyses showed that S129A-expressing dopaminergic neurons enclosed numerous α-syn-positive electro-dense cytoplasmic aggregates (Fig. 3A–C). Higher magnification of some of these relatively small cytoplasmic, fuzzy and amorphous structures indicated the possible presence of filamentous material. Aggregates appeared also in some dopaminergic neurons transduced with WT, A30P or both S129D and A30P/S129D variants, although to a much lesser extent (Fig. 3C).

Fewer but larger aggregates in the case of S129D

Our overall appraisal, with fluorescence microscopy, was that ThioS-fluorescent structures in the S129D brains were less numerous, but generally larger in size than those observed in the other groups (Fig. 4A). In order to examine this observation in a more quantitative manner, we first scanned with a confocal microscope up to 110 whole ThioS-positive nigral neurons of rats injected with the A30P variants. Multichannel, three-dimensional images of 178 ThioS-positive aggregates were deconvolved and processed through an image analysis software of volumetric segmentation, and quantitative data were extracted with the ImageJ program. As the amplification of the signal generated by fluorescence is to be taken into account (34), we did not regard crude values put forth by the ImageJ computational program as scale-sensitive measures.

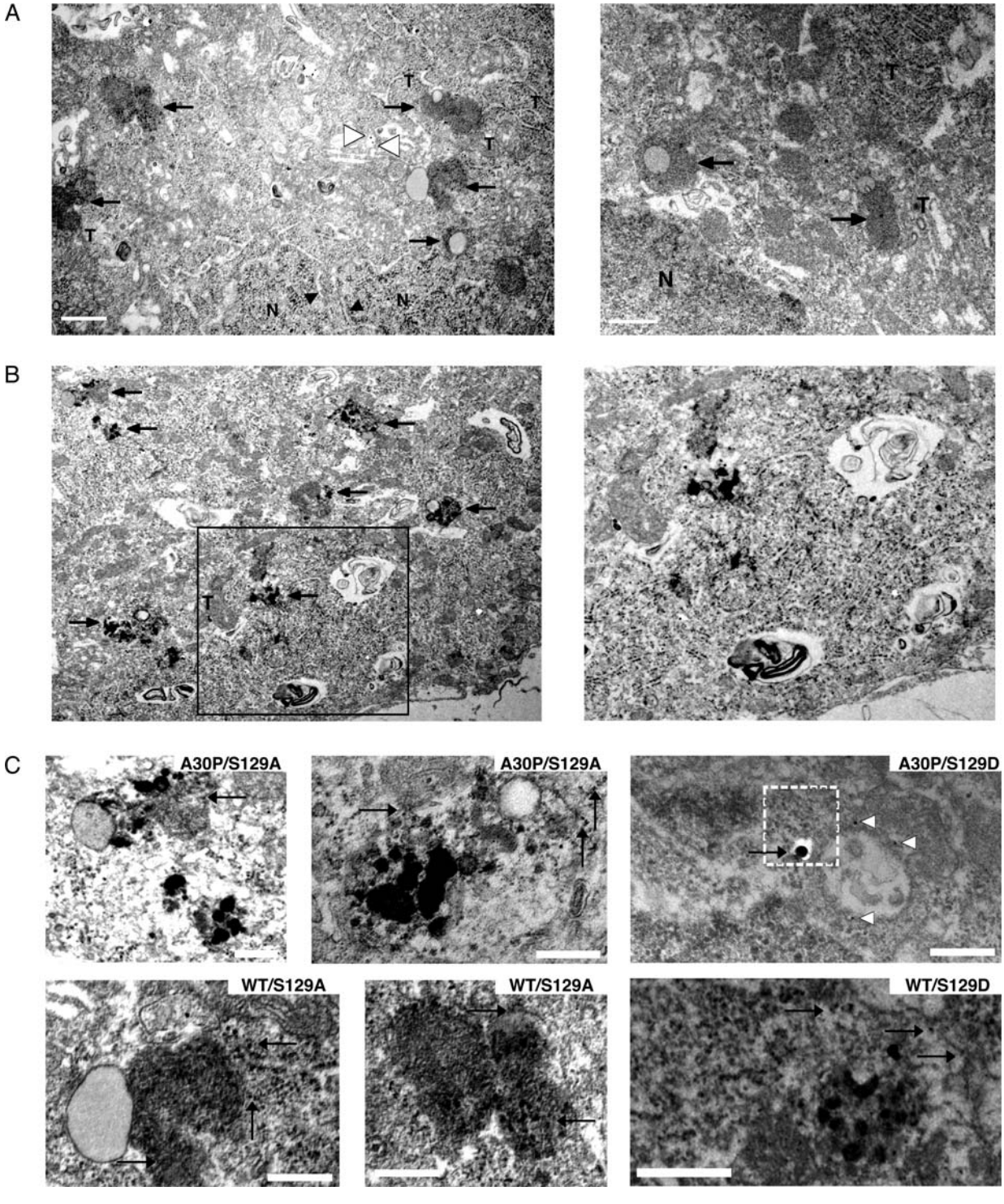

Figure 3. IEM demonstrating α-syn-positive aggregates and extensive nigral human α-syn-positive staining. Numerous α-syn-positive electro-dense cytoplasmic aggregates (arrows) in the nigral neurons expressing the WT/S129A variant (**A**) and the A30P/S129A variant (**B**), mostly positioned in the vicinity of the nucleus (N) and of tubulo-membranous structures (T)—the ER and the Golgi apparatus. (A) Black arrowheads indicate the lobulation of the nucleus. White arrowheads indicate stained Golgi cisternae. (B) Box: magnification of a tubulo-membranous structure, probably the ER. (**C**) Higher magnifications of WT/S129A, A30P/S129A, WT/S129D and A30P/S129D aggregates. These higher magnifications reveal filamentous material at times (arrows and white box), association with lysosomes (dark flecks) and with a phagosome-like halo structure containing vesicles. Gold particles are visualized in the filamentous material and near to the membrane enclosing vesicles (white arrowheads). Scale bars (B): 500 nm and (C): 250 nm.

However, as all slices were treated simultaneously under strictly the same conditions and image acquisition and deconvolution were performed with the exact same parameters, we could give credence to the relative differences among the groups. In fact, measures indicated that the mean volume of a single signal yielded in A30P/S129D-injected animals was

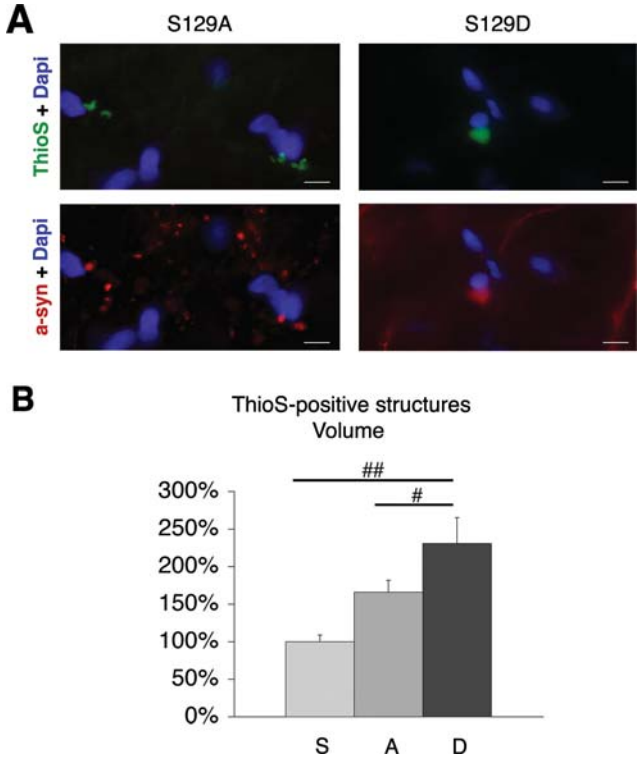

Figure 4. S129D-expressing rats display larger α-syn-, ThioS-positive aggregates. (**A**) ThioS signals, colocalizing with α-syn staining, adjoining the nuclei. ThioS-positive structures in the S129D-injected brains appear generally larger in size than those observed in S129A-injected brains. Scale bars, 10 μm. (**B**) Volumetric segmentation analysis of three-dimensional deconvolved images of 178 ThioS-positive aggregates. The mean volume of a single signal yielded in A30P/S129D-injected animals was 1.4- and 2.3-fold that of signals yielded in A30P/S129A and A30P animals, respectively (A30P-injected rats: $n = 4$; A30P/S129A-injected rats: $n = 6$; A30P/S129D-injected rats: $n = 6$). $^{\#}P < 0.05$ and $^{\#\#}P < 0.0001$. Data were expressed as average ± SEM.

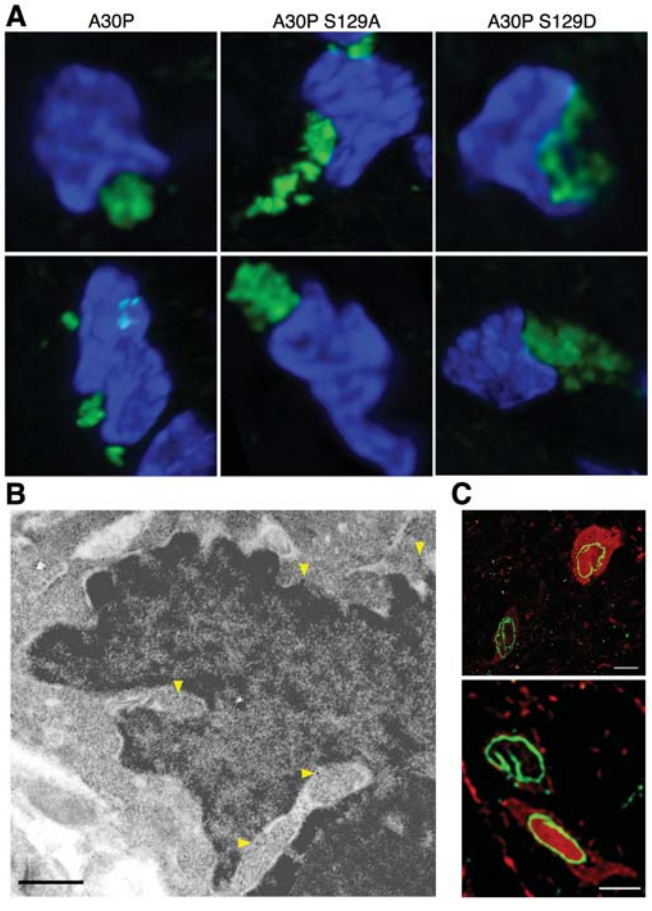

Figure 5. Condensation and lobulation of the α-syn-positive neuronal nuclei. (**A**) Confocal images of neurons stained with ThioS (green) and Dapi (blue), illustrating the condensation and irregularity in shape of cells bearing ThioS-positive structures. ThioS-positive signals are most frequently arrayed in the vicinity of the nucleus and clearly mark the indented regions of the irregularly shaped nucleus. Scale bars, 2 μm. (**B**) IEM images of neurons within the SN pars compacta. Note the extensive α-syn-positive staining in-between the lobulations (yellow arrowhead). Rats injected with WT/S129A. Scale bars: 500 nm. (**C**) Immunohistological co-staining against lamin-B-positive nuclear membranes (green) and human α-syn (red). Note the correlation between lobulated nuclei and enhanced punctation in α-syn signals. Scale bars: 5 μm.

1.4- and 2.3-fold that of signals yielded in A30P/S129A and A30P animals, respectively (Fig. 4B). These data suggest that the process of aggregation in the case of the S129D variants differs from that in the case of the other variants.

Subcellular events providing insight into how preventing phosphorylation enhances the cytotoxicity of α-synuclein

IEM images revealed that aggregated α-syn-positive structures were frequently associated with lysosomes, which appeared as dark flecks in the IEM images. These aggregates were often associated with a round, glassy and unstained phagosome-like structure. Vesicular content was discernible in some of these structures (Fig. 3C). IEM also showed that the aggregates preferentially localized in the perinuclear region and were also often neighboring intracytoplasmic membranes. This was in agreement with the results obtained by confocal scanning, which illustrated that ThioS-positive signals were most frequently arrayed in the vicinity of the nucleus and clearly marked the indented regions of the irregularly shaped nucleus (Fig. 5A). S129A- and A30P/S129A-expressing neurons differed from the other groups, in that they displayed extensive positive staining in tubulo-membranous structures (Fig. 3)—the endoplasmic reticulum (ER) and the Golgi apparatus (Figs 3A and 6A)—as well as in the outer membrane of the mitochondria (Fig. 6B). Alpha-syn was much less present in intracellular membranes in the intact Ser129- and S129D-expressing nigral neurons. In these groups, the association of α-syn with the membranous tubular system occurred only with the formation of aggregated structures. Finally, in S129A groups, IEM showed a large amount of gold particles associated with a disarrayed network of neurofilaments in neuritic fibers (Fig. 6C).

Nuclear localization correlates with enhanced toxicity of α-synuclein species rather than being associated with phosphorylation

As phosphorylated α-syn was found to be preferentially localized in the nuclei of some dopaminergic neurons in synucleinopathy models (35–38), we investigated the existence of a

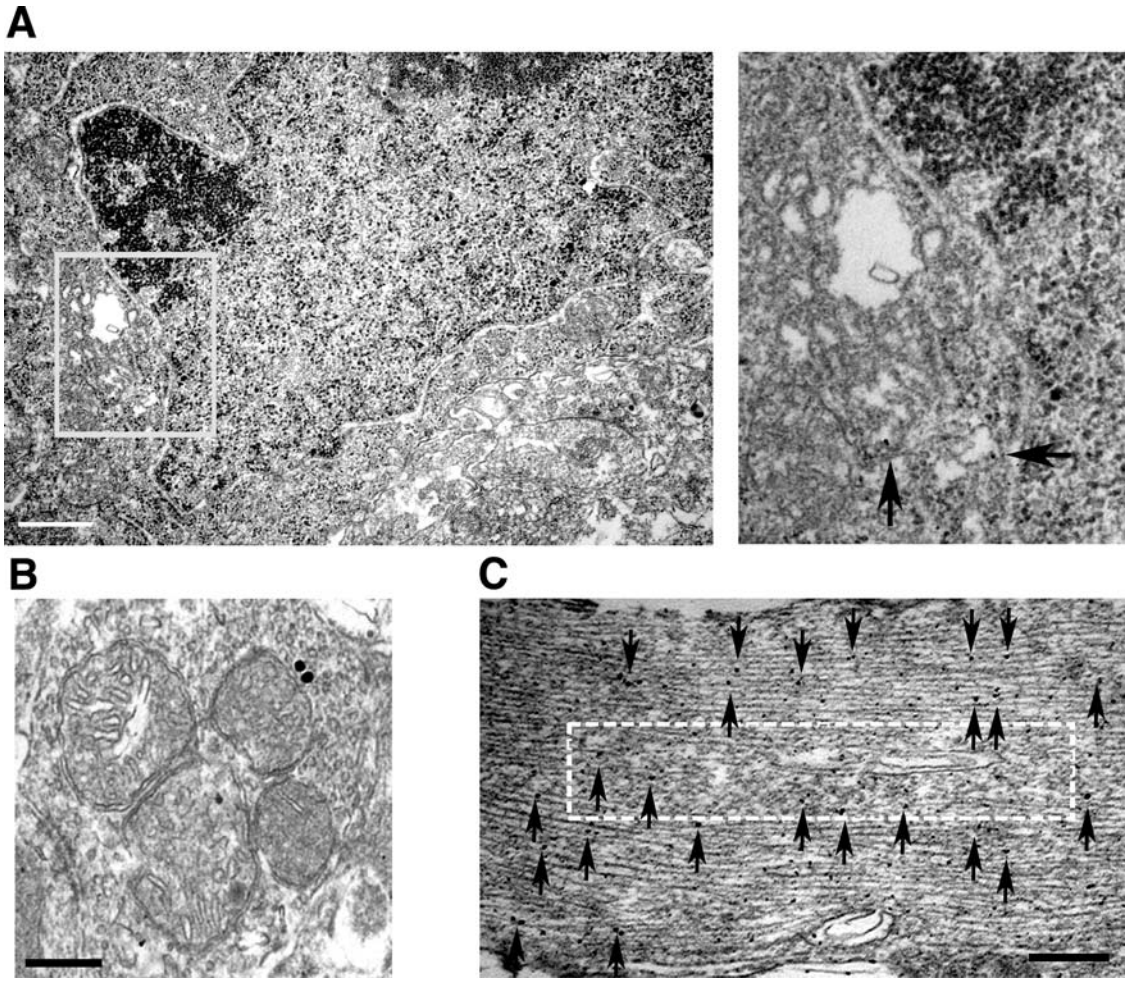

Figure 6. IEM demonstrating labeling of the Golgi apparatus, mitochondria and neurofilaments. (**A**) Positive staining of the Golgi apparatus. Rats injected with WT/S129A. Box: magnification of stained cisternae (arrows). (**B**) Gold particles on the outer membrane of mitochondria. Rats injected with A30P/S129A. (**C**) Extensive staining of neurofilaments within a neuritic fiber (arrows) and disarrayed network of stained neurofilaments (white box). Rats injected with WT/S129A. Scale bars: (A) 500 nm, (B) 250 nm and (C) 200 nm.

correlation between the phosphorylation status at serine 129 and nuclear localization of the protein. Triple immunostaining with the use of an antibody specifically recognizing human α-syn, PSer129 antibody (1) and an antibody recognizing lamin-B in brains injected with WT or A30P α-syn confirmed phosphorylation in these rats and disclosed intense fluorescence within the nuclei (Fig. 7A and B). Phosphorylated α-syn was also present in neuronal processes, in which it accumulated in beaded formations. In S129A- and S129D-expressing neurons, fluorescent staining with the use of a phosphorylation-independent antibody against human α-syn showed expression in the cytoplasm and the nucleus, as well as in the neuritic processes (Fig. 7C). However, in the S129A forms, there were more beaded formations in the fibers and, within the cell body, α-syn's fluorescence was more intense in the nucleus, when compared with the other forms. Strikingly, nuclear staining was also positive in the S129A-expressing cells analyzed by IEM, which revealed extensive numbers of gold particles in the S129A neuronal nuclei when compared with the serine forms and S129D variants (Fig. 7D and E). These observations strongly suggest that rather than being associated with phosphorylation, nuclear localization correlates with enhanced toxicity of the α-syn species.

Activation of Bax and caspase-9 and morphological characteristics of apoptosis in cells developing aggregates

Ongoing nigral neurodegeneration was demonstrated in the A30P- and A30P/S129A-injected rats by positive staining against cleaved caspase-9 and Bax (Fig. 8A and B). Strikingly, these markers were also activated in the A30P/S129D-injected rats (Fig. 8C). Co-staining of cleaved caspase-9 and dopaminergic-specific TH marker showed that the apoptotic pathway was activated in the remaining dopaminergic neurons. The activation of these markers of apoptosis substantiates the assumption that the significant decrease in TH-positive nigral neurons was due to cell death rather than to TH down-regulation.

In parallel, we observed morphological markers of apoptosis: IEM and immunofluorescence analyses called attention to the fact that, in all variants, nuclei of neurons displaying

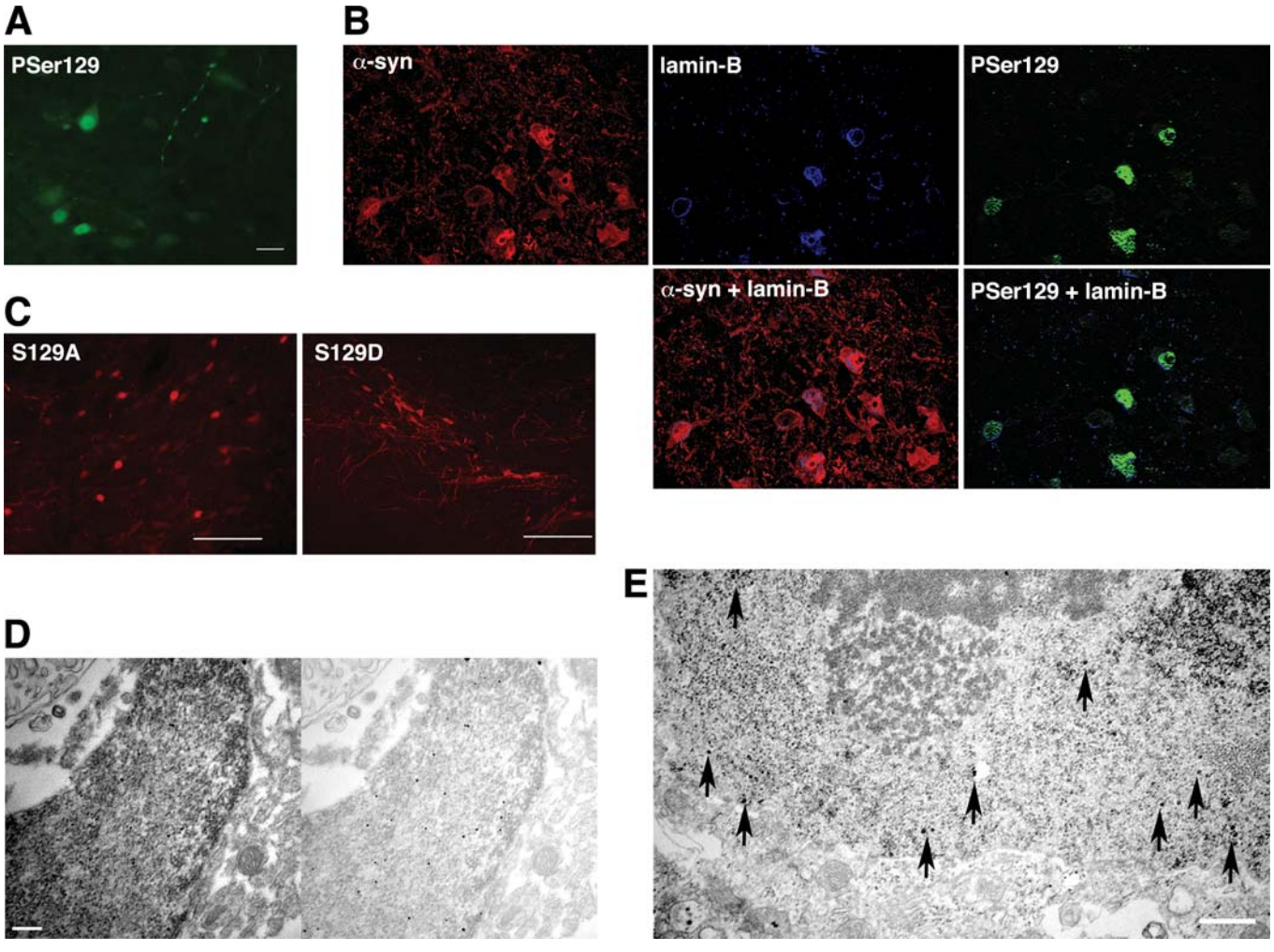

Figure 7. Enhanced nuclear localization of α-synuclein neurotoxic species. (**A**) Immunostaining with PSer129 antibody reveals enhanced localization in nucleus as well as accumulation along neural processes. Scale bar: 20 μm. (**B**) Confocal images of neurons in the SN of rats injected with A30P. Immunohistological co-staining against human α-syn (red), phosphorylated α-syn (green) and lamin-B (blue). (**C**) Immunostaining with the phosphorylation-independent antibody against human α-syn reveals intensified nuclear localization of S129A when compared with S129D. Note the concomitant, widespread presence of S129A in the fibers. Scale bars: 200 μm. (**D** and **E**) IEM images revealing numerous gold particles in the WT/S129A (C) and A30P/S129A (D) neuronal nuclei. Scale bars: (C) 500 nm and (D) 200 nm.

aggregates were condensed and lobulated (Fig. 5). Lobulation was perceived with the use of lamin-B staining against the nuclear membrane (Fig. 5C). Remarkably, cells displayed lobulated nuclei in correlation with punctate α-syn-positive signals and were less lobulated when α-syn staining was diffuse. Moreover, confocal images processed through the ImageJ segmentation software revealed that the mean volume of nuclei, stained with Dapi, in cells displaying ThioS signals, was reduced by 40%, and their mean Dapi-fluorescence intensity was enhanced by 180% when compared with the nuclei of ThioS-negative neurons.

DISCUSSION

The question of the role of phosphorylation of α-syn in the pathogenic process of PD remains a debated issue. Various *in vitro* and *in vivo* results are divergent (1,30,31,39–43). In the present work, we combined several approaches to explore the cellular events underlying the impact of phosphorylation of human WT and A30P α-syn expressed in the nigral dopaminergic neurons of rats. In agreement with results obtained in a previous study of rAAV-injected rats (31), the expression of the phosphorylation-prevented S129A variants exacerbates α-syn toxicity, whereas the expression of the phosphorylation-mimicking S129D variants does not cause dopaminergic deficits.

Our quantitative investigation reveals that significantly higher numbers of α-syn aggregates are formed in the SN of rats injected with the most neurotoxic form, S129A, in a dose-dependent manner and independent of the presence or absence of the familial A30P mutation. The correlation between dopaminergic cell loss and enhanced formation of relatively small aggregates supports the hypothesis that aggregated α-syn species, precursors of the characteristic inclusions of PD, are intimately linked with the progression of nigrostriatal degeneration. In line with these observations, S129D-injected animals, which do not present any significant nigral neuronal loss,

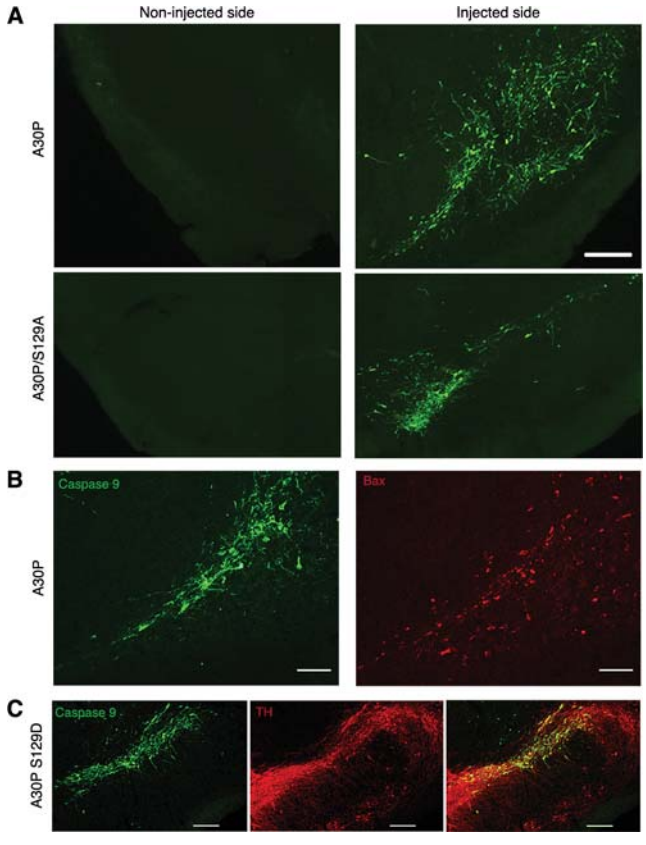

Figure 8. Markers of apoptosis are activated. (**A**) Positive immunostaining against activated caspase-9 revealed on the injected SN of A30P and A30P/S129A rats, in contrast to the non-injected side. Scale bars: 200 μm. (**B**) Co-immunostaining of activated caspase-9 (green) and Bax (red), as illustrated here in an A30P rat. Scale bars: 100 μm. (**C**) Caspase-9 is also activated in A30P/S129D rats. Co-immunostaining of activated caspase-9 (green) and TH marker (red). Scale bars: 200 μm.

indeed display a significantly lower amount of aggregates. The SN of S129D-injected rats are however not devoid of aggregates when compared with the contralateral non-injected SN, where virtually no signal can be detected.

The above data challenge two recent propositions. First, it has been proposed by various investigators that the expression of the S129A mutant protein leads to fewer inclusions (31,40,43). The present immunohistological and biochemical analyses reveal that the expression of the S129A mutant leads to the formation of significantly higher amounts of aggregates. The aggregates are ThioS-positive, indicating the formation of β-sheet-rich α-syn aggregated structures in the neuronal cell body and in processes as well. They are also PK-resistant, and IEM reveals that they are irregularly shaped, associated with specific organelles and positioned in the vicinity of the nucleus. Secondly, the estimation of dopaminergic nigral cell loss, which is significantly higher following S129A expression, when compared with S129D expression, has led to the suggestion that phosphorylation protects from neurodegeneration (31). Evidence is provided here that aggregates are formed and signals of apoptosis are activated also in rats expressing the S129D form of α-syn. Hence, phosphorylation-mimicking variants of α-syn—both the WT form and the A30P mutant—cannot be considered protective.

The enhanced aggregation and cytotoxicity of the S129A variants are all the more surprising in view of the well-described presence of phosphorylated α-syn almost exclusively in the insoluble fraction of synucleinopathic human brains. The following explanation can be advanced. Phosphorylation intervenes in the conversion from fibrils to inclusion bodies. Preventing phosphorylation hinders the agglomeration of fibrils into inclusion bodies, thereby causing the accumulation of the cytotoxic early stage aggregated species. This is supported by our observation that the few aggregates developed in the S129D groups are larger than those in the S129A groups. Another possible explanation is that phosphorylation of α-syn is not a direct cause of pathology. Rather, phosphorylated α-syn is detected in inclusions because, as already shown for some proteins (44–46), phosphorylation may act as a signal for elimination. In the pathological situation of PD, the proteolytic machinery of elimination is impaired. If phosphorylation indeed regulates the turnover of α-syn, in PD cases, phosphorylated α-syn accumulates in the cytoplasm, is entrapped in the course of aggregation and is thus found abundant in the inclusions. In our model, the expression of the phosphorylation-prevented S129A variants forestalls the signal for the normal turnover of the protein. These variants then mediate degeneration via the formation of toxic pre-inclusion aggregates, via enhanced affinity for membranes and via nuclear localization.

A closer analysis of α-syn-positive staining and of the electro-dense aggregates reveals a number of cellular events and provides a mechanistic insight into the mediation of acute toxicity by α-syn S129A. Interestingly, these data correspond to cellular events pointed out in post-mortem investigations of human cases and therefore give weight to the validity of the rAAV-based rodent model of PD expressing human α-syn (31,38,47–49).

First, we found that dark lysosomal bodies and phagosome-like glassy bodies are most often trapped in the relatively small aggregates. In fact, α-syn can be cleared by autophagy (50–53), and autophagic lysosomal impairment is known to participate in the amyloidogenic aggregation of α-syn (51,54–56). Reciprocally, the expression of mutant α-syn in rat ventral midbrain cultures blocks lysosomal function (51). The sequestration of lysosomes and phagosomes could be a consequence of the attempt of cells to remove abnormal aggregated proteins and damaged organelles from the cytoplasm.

Secondly, in our model, we observe the prominent presence of α-syn in the vicinity of the nucleus, particularly in the indented regions of the nucleus, and we witness the accumulation of the protein in intracytoplasmic membranes, particularly in tubulo-membranous structures—the ER and Golgi apparatus. This is in line with the currently dominant hypothesis that phosphorylation of α-syn reduces the interaction of the protein with phospholipids (1,38,42). This hypothesis, however, has led some to suggest that decreased affinity of phosphorylated α-syn for membranes leads to an increase in the free α-syn pool, thereby contributing to promote its assembly into abnormal filaments in the cytoplasm. We rather demonstrate the enhanced neurotoxic potential of the phosphorylation-prevented variants.

On the one hand, our observations described earlier indicate impairment in ER–Golgi trafficking. Cellular models of PD

showed that α-syn accumulation correlates with induced disruption of the ER–Golgi vesicular trafficking and ER stress (57–59). The pathogenic expression of α-syn has also been shown to disrupt the ubiquitin-dependent proteasomal system, which may be responsible for the accumulation of misfolded protein in the ER and may contribute to enhanced vulnerability to ER stress. The upregulation of ER stress markers and fragmentation of the Golgi apparatus were reported in several human neurodegenerative diseases (60–64). ER stress has been functionally correlated with accumulated and aggregated α-syn and identified as a pathogenic event present in dopaminergic neurons of PD cases (57,65,66). Interestingly, a cellular study of PD reported strong correspondences between prefibrillar aggregate-forming α-syn in the perinuclear region, Golgi fragmentation and aggregation of intact and active lysosomes, mitochondria and autophagosome precursors, at the inclusion-forming sites (67).

On the other hand, damage of the Golgi apparatus could result from the impaired, overloaded microtubule-mediated transport system (68). Indeed, our IEM analysis indicates the extensive amount of gold particles associated with a disarrayed network of neurofilaments in neuronal processes of S129A-injected rats. We noted also Lewy-like dystrophic neurites with the appearance of α-syn- and ThioS-positive beaded formations along neuronal processes. The accumulation of α-syn species along the trafficking system may therefore indirectly contribute to Golgi fragmentation, which is linked to apoptosis (69,70). Consistent with our observations, post-mortem analyses of PD brains showed that Golgi fragmentation is mostly induced in nigral neurons bearing precursors of inclusion bodies, when compared with neurons containing Lewy bodies (71).

Thirdly, we report, in our S129A model, the association of α-syn S129A with the outer membrane of mitochondria and we witness in all variants the activation of Bax and caspase-9, which are intimately linked to mitochondrial damage (72). It is reasonable to believe that the presence of α-syn interferes with the mitochondrial respiratory chain system. Indeed, a number of *in vitro* studies have demonstrated the association of α-syn with mitochondrial membranes (73–75) and have proposed this association has a pivotal role in the pathogenesis of PD, as it provokes the release of cytochrome *c* with the subsequent activation of caspase cascade and with oxidative damages, eventually causing apoptosis (72,74). In addition, a recent analysis of mitochondria from the SN and striatum of post-mortem late-onset PD brains also reported significant association of α-syn with mitochondria and with complex I as well as decreased complex I activity (76). This will be enhanced when α-syn oligomers and protofibrils are involved. Mitochondrial pathology was reported in cell cultures overexpressing α-syn as well as in transgenic mice overexpressing the A53T α-syn mutant (57,58,61,67,77–80). Mitochondrial activity was estimated to decrease by 30–40% in the SN of PD brains (81–84). As for markers of apoptosis, activation of Bax-dependent pathways and of apoptotic effectors caspase-3 and -9 has been identified in correlation with nigral dopaminergic cell loss in PD (85–87). These pathways contribute to nuclear chromatin condensation and DNA fragmentation, which have become morphological hallmarks of apoptotic degradation (88). Remarkably, we observed in both S129A- and S129D-injected rats that nuclei of dopaminergic neurons displaying aggregates are condensed and lobulated. Furthermore, susceptibility to α-syn overexpression appears to be specific to neurons, because IEM analysis reveals that oligodendroglial cells, which also express human α-syn, never present lobulated nuclei nor aggregates (data not shown).

Fourth, our observations indicate that enhanced toxicity of S129A correlates with intensified nuclear localization. The detection of intense and diffuse staining in the S129A nuclei was unexpected in view of studies reporting preferential localization of phosphorylated α-syn in the nucleus of some dopaminergic neurons in synucleinopathy models (35–38). Our results show that it is not phosphorylation that prompts localization to the nucleus. Nuclear localization rather correlates with enhanced toxicity of α-syn species. In fact, increased nuclear localization has been associated with increased toxicity in PD according to experiments revealing α-syn interaction with histones (36,89,90).

In our experimental design, the expression of WT α-syn or of the α-syn A30P mutant leads to a rather modest loss of dopaminergic neurons. In order to discuss our results and position them with respect to previous studies, we performed western blot analyses to assess the level of expression, and we were able to compare values. Our experimental design leads to an approximate doubling of the total amount of α-syn in the SN. This result is pertinent in many ways. Alpha-syn transgenic mice have been described to express 2–15 times the level of the endogenous protein, but none of them displayed significant nigrostriatal degeneration (7,91–94). The mild neuropathology in these mouse models has been explained either by species specificities or by compensatory responses arising with constitutive overexpression of α-syn during development, or finally by the assumption that a critical threshold of α-syn expression is required for triggering nigrostriatal dopaminergic degeneration and behavioral defects. Our model demonstrates that the acute induction of α-syn expression in adult rats, only doubling the nigral expression of α-syn, is sufficient to trigger significant nigral cell loss. Furthermore, we used lower amounts of viral vectors, leading to a lower extent of neurodegeneration, for the purpose of avoiding non-specific effects and inflammatory responses provoked by an excessive concentration of viral particles. Our results correlate with another study (31), in which rAAV injection of WT α-syn led to an approximately 3.6-fold increase in total α-syn expression and to ∼40% loss of TH-positive nigral neurons. Our rAAV2/6 injection of WT α-syn causes a ∼20% loss of TH-positive nigral neurons. It is interesting to note that an approximate doubling of WT α-syn expression has been reported in the case of several families with α-syn genomic multiplication and developing an autosomal-dominant PD (12,15,95,96). Furthermore, our results show that a doubling of the total level of α-syn displays higher toxicity than the A30P missense mutant. In agreement with our observations, an excess of WT α-syn was reported to have more devastating consequences than mutant α-syn (12). An approximate doubling in α-syn expression appears to be a major determinant of the age of onset, the extent of the neurodegenerative process and the severity of the phenotype (12,15,96,97).

Our data show that aggregates and morphological characteristics of cell death are present in all rats—expressing either phosphorylation-mimicking or phosphorylation-preventing α-syn variants—although they appear with distinct intensities or at different paces. We suggest that the different mutant forms activate mechanisms with distinct dynamic properties. Besides, phosphorylation of serine at position 87 (Ser87), which has a critical position within the NAC domain, was pointed out *in vitro* (98–100). *In vivo* analyses of the potential of phosphorylation at Ser87 may complement the understanding of the impact of this post-translational modification on the properties of α-syn in PD pathogenesis. The modulation of phosphorylation of α-syn by the use of kinases or phosphatases has been a candidate in the development of therapeutic tools. Our results bring a new perspective to these strategies for the treatment of PD. The uncovering of the subcellular structures involved in the process of neurodegeneration may also contribute to a better understanding of the important presymptomatic phase of the disease and to the development of neuroprotective therapies.

MATERIALS AND METHODS

Plasmid construction

Human WT and human A30P α-syn genes (nucleotides 46–520, GenBank accession no. NM_000345) were cloned into the AAV-CMV-MCS (Stratagene, La Jolla, CA, USA) backbone. Single-nucleotide mutations were introduced to the human WT and A30P α-syn genes using QuickChange Site-Directed Mutagenesis Kit (Stratagene): replacement of a T at position 385 of the sequence of human α-syn by a G yielded an S129A mutation. Replacement of a C at position 386 of the sequence of the S129A variant by an A yielded an S129D mutation. Primers used for the generation of the S129A variants were sense: TATGAAATGCCTGCTGAGG AAGGGTAT and antisense: ATACCCTTCCTCAGCAGG CATTTCATA and for the generation of S129D variants were sense: GAAATGCCTGATGAGGAAGG and antisense: CCTTCCTCATCAGGCATTTC.

rAAV2/6 virus production and titration

The recombinant pseudotyped rAAV2/6 (rAAV2 genome packaged in the serotype 6 capsid) was produced by co-transfecting the pAAV-CMV shuttle plasmid coding for α-syn with the pDF6 packaging plasmid (101). Cell lysate was subjected to purification by high-performance liquid chromatography on the HiTrap Heparin column (GE Healthcare Bio-Sciences AB, Uppsala, Sweden). The viral suspension obtained was concentrated by using Centricon Plus-20 filter units (Regenerated Cellulose 100,000 MWCO; Millipore, Billerica, MA, USA), and the suspension medium was replaced with phosphate-buffered saline (PBS). The viral genome (vg) titers were then evaluated. A defined volume of viral suspension (1 μl) was digested with PK (10 mg/ml) at 55°C for 30 min. The number of vg/ml was determined by real-time polymerase chain reaction (PCR) using a set of primers specific for a viral sequence in the beta-globin intron (forward: CGTGCCAAGAGTGACGTAAG and reverse: TGGTGCAAAGAGGCATGATA). In order to measure the relative infectivity of all viruses, human embryonic kidney 293T cells were infected with serial dilutions of viruses. Forty-eight hours later, cells were collected and total DNA was extracted using DNeasy Blood&Tissue Kit (Qiagen, Valencia, CA, USA) according to the supplier's protocol, including the optional RNase A treatment. Then, in order to eliminate transcriptionally inactive single-stranded viral genomes, extracted DNA was treated with S1 nuclease (Promega, Madison, WI, USA) at a final concentration of 60 U/ml for 30 min at 37°C. The enzyme was inactivated for 15 min at 97°C. Samples were again purified on DNeasy columns to remove buffer components that interfere with real-time PCR reaction. The number of remaining viral genomes was finally measured by real-time PCR using the beta-globin primers described earlier. In parallel, the amount of cellular DNA was determined using a pair of primers specific for the human albumin gene (forward: TGAAACATACGTT CCCAAAGAGTTT and reverse: CTCTCCTTCTCAGAAA GTGTGCATAT). This permitted to take into account the total input of target cells. Relative infectivity of viruses was calculated by plotting the logarithm of beta-globin copies (corrected for the albumin content) against the logarithm of virus dilutions. The plot was used to determine the dilution interval between viruses, which was subsequently converted into a relative infectivity ratio. TUs were then estimated by comparison with a reference AAV vector [AAV-CMV-EGFP (Enhanced Green Fluorescent Protein)], whose infectivity was determined by flow cytometry for direct EGFP fluorescence. The percentage of EGFP-positive cells was determined 48 h after infection of 293T cells, with respect to non-infected control cells and the number of infection events calculated according to Poisson's formula. The estimated titer of the AAV-CMV-EGFP viral batch was 2×10^{10} TU/ml. The titer measures obtained were the following: AAV-CMV-α-syn-WT: 1.7×10^{11} TU/ml, AAV-CMV-α-syn-WT-S129A: 1.2×10^{11} TU/ml, AAV-CMV-α-syn-WT-S129D: 1.7×10^{11} TU/ml, AAV-CMV-α-syn-A30P: 0.9×10^{11} TU/ml, AAV-CMV-α-syn-A30P-S129A: 1.9×10^{11} TU/ml and AAV-CMV-α-syn-A30P-S129D: 1.4×10^{11}TU/ml.

In vitro expression

293T cells were infected with 2 μl of rAAV2/6 vectors, and cellular lysates were harvested 2 days post-infection in lysis buffer (Tris buffer saline, EDTA 1 mM, Triton X 0.5%, NP40 0.5%) containing protease inhibitors (Roche Pharma, Basel, Switzerland). The lysis buffer included additional okadaic acid (10 μM) and sodium orthovanadate (0.5 mM) for experiments to detect the presence of phosphorylated α-syn. Equal amounts of protein (50 μg) were loaded onto 15% sodium dodecyl sulfate (SDS)–polyacrylamide gel (PAGE), followed by the transfer of proteins onto a nitrocellulose membrane (Bio-Rad, Hercules, CA, USA). A polyclonal antibody generated against the 101–124 amino acid sequence of human α-syn was generated and affinity-purified with the immunogen by Research Genetics (Huntsville, AL, USA) and used to detect the α-syn protein (1:1000). An anti α-syn phosphorylated at Ser129 (1) was used to detect phosphorylated α-syn. Equal total protein load was checked by probing the same membrane

with an anti-tubulin antibody (1:2000; Sigma, St Louis, MO, USA). Detection and quantification were performed using the Odyssey® Infrared Imaging System.

Stereotaxic unilateral injection into the SN of rats

Adult Wistar female rats (Charles River Laboratories, France) weighing ~200 g were housed in 12 h light/dark cycle, with *ad libitum* access to food and water, in accordance with the European Community Council directive (86/609/EEC) for the care and use of laboratory animals. For stereotaxic injections, the animals were deeply anesthetized with a mixture of xylazine/ketamine and placed in the stereotaxic frame (David Kopf Instruments, Tujunga, CA, USA). Two microliters of viral preparation were injected in the right brain hemisphere of these rats using a 10 μl Hamilton syringe with a 34-gauge blunt tip needle at a speed of 0.2 μl/min, with an automatic pump (CMA Microdialysis, Sweden). The needle was left in place for an additional 5 min before being slowly withdrawn. SN was targeted by using the following anterior, lateral and ventral coordinates: 5.2, 2.0, 7.8 mm (bregma coordinates) (according to the atlas of Paxinos and Watson).

Human α-synuclein extraction from SN samples

Eight weeks post-injection, three rats per group were sacrificed using a guillotine. Their brains were then rapidly extracted and immediately frozen in cold isopentane and stored at −80°C. SN cryosections (Leica CM 3050S, Leica, Nussloch, Germany) were homogenized in a Tris buffer (Tris–HCl 50 mM, NaCl 150 mM, EDTA 2 mM, EGTA 2 mM, 10% sucrose) containing 1 mM dithiothreitol, 0.5 mM Na_3VO_4, 100 nM okadaic acid and protease inhibitors (Roche Pharma) and centrifuged at 130 000*g* for 1 h at 4°C. Protein concentration was determined by the BCA Protein Assay Kit (Pierce, Rockford, IL, USA). Equal amounts of protein (50 μg) were loaded onto 15% SDS–PAGE, followed by the transfer of proteins onto a nitrocellulose membrane (Bio-Rad). A sheep anti-α-syn antibody (AB5334P, Chemicon, Temecula, CA, USA) recognizing both human and rat α-syn was used to assess the level of expression of the transgene when compared with the endogenous protein. The amount of protein loaded was checked on the same membrane with an anti-actin antibody (sc-1616, Santa Cruz Biotechnology, Santa Cruz, CA, USA). Detection and quantification were performed using the Odyssey® Infrared Imaging System.

Immunohistological analyses and counting

Eight weeks post-injection, rats were deeply anesthetized by an overdose of pentobarbital and perfused transcardially first with PBS and then with ice-cold 4% paraformaldehyde (PFA, Fluka-Sigma, Buchs SG, Switzerland). Brains were kept for 90 min in 4% PFA and then transferred to 25% sucrose. Twenty-five μm-thick coronal sections from both the SN and the striatum were harvested on a sliding microtome (Leica SM2400; Leica) at a temperature of −20°C. Slices were then processed for immunohistological treatment.

For immunofluorescence studies, slices were washed in PBS before blocking in a solution of 10% normal donkey serum (NDS) (Jackson ImmunoResearch, Suffolk, UK), 1% albumin from bovine serum (BSA, Fluka-Sigma) and 0.1% Triton X-100 in PBS, during 2 h at room temperature. Slices were then incubated overnight at 4°C with the primary antibodies in blocking buffer and subsequently incubated for 2 h at room temperature in a mix of secondary antibodies conjugated with 488- and/or 568-Alexa Fluor dyes (Molecular Probes, Invitrogen AG, Basel, Switzerland) and 1% NDS, previously centrifuged at 10 000*g* for 20 min at 4°C. Slices were finally washed and mounted on glass slides using a DABCO-glycerol mounting solution. The primary antibodies used in this study are: anti-human α-syn monoclonal antibody (LB509; Zymed, San Francisco, CA, USA), anti-α-syn phosphorylated at Ser129 (1), anti-lamin-B (sc-6217, Santa Cruz Biotechnology), anti-cleaved caspase-9 (rat-specific, Asp353; Cell Signaling Technology, Beverly, MA, USA), anti-Bax (6A7; BD Biosciences, Clontech, San Diego, CA, USA), anti-TH (Chemicon) and anti-VMAT2 (AB1767, Chemicon). Double immunofluorescence staining was performed by simultaneous incubation of sections with the two primary antibodies, followed by the two secondary antibodies. For double α-syn-thioflavin S (ThioS) staining, α-syn immunofluorescent staining was preceded by the following steps: slices were washed in water, incubated for 20 min in 0.05% ThioS diluted in 50% ethanol and filtered, differentiated in three washes of 5 min each in 80% ethanol and finally extensively washed in PBS. Dapi staining was performed by incubating the slices in 4′,6-diamidino-2-phenylindole (Dapi) at a concentration of 1 μg/ml diluted in water for 12 min followed by substantial washing in PBS.

Percentage of neurons positive for dopaminergic markers [use of an anti-TH antibody (1:500) and an anti-VMAT2 antibody (1:2500)] relative to the contralateral non-injected side was determined by counting 24 coronal sections (one in six sections) throughout the SN, under a light microscope (Olympus CX41) at a magnification of 200×. Striatal dopaminergic innervation was analyzed by quantifying the OD of TH- and VMAT2-immunoreative terminals in 16 (one in six sections) striatal sections, relative to the contralateral non-injected hemisphere. These sections were scanned using a Nikon Super Coolscan 4000 scanner, and the OD of the tissue (OD that corresponds to the integrated density of gray values of pixels with correction for non-specific background) was analyzed using the ImageJ software (free NIH software: http://rsb.info.nih.gov/ij/). ODs were measured bilaterally through all the striatum, and arbitrary units were assigned. The number of ThioS-positive aggregates per mm^2 was obtained by counting two sections at an antero-posterior coordinate of −5.2 (bregma coordinates), at a 40× magnification. All analyses were performed in a blinded fashion.

For the staining of human α-syn resistant to PK, slices were first washed in PBS and mounted on Superfrost Plus glass slides (Menzel-Glaser GmbH&Co KG, Braunschweig, Germany). Dried mounted slices were incubated for 15 min in PK 10 μg/ml diluted in 0.1 M Tris–HCl buffer, pH 7.5, 5 μM EDTA at room temperature. After PBS washes, slices were quenched with 0.1% phenylhydrazine (Merck, Whitehouse Station, NJ, USA) in PBS at 37°C for 1 h and incubated for 2 h at room temperature in a blocking solution of 10% horse serum (HS) [Amimed (Bioconcept), Switzerland], 1% BSA (Fluka-Sigma) and 0.1% Triton X-100 (Sigma) in PBS. Overnight incubation with an anti-human α-syn monoclonal

antibody (LB509; Zymed) in blocking buffer at 4°C was followed by a 2 h incubation with biotinylated goat anti-rabbit immunoglobulins (Vector Laboratories, Burlingame, CA, USA) and subsequently by incubation in avidin–biotin–peroxidase solution (Vector Laboratories) for 30 min. Slices were finally revealed with 3,3′-diaminobenzidine solution (DAB) (Pierce) and mounted on glass slides.

Image processing and analysis

Observations, counting and brightfield image acquisition were obtained on a Leica DMI 4000 microscope (software: Leica LAS) using an Olympus AX70 color camera. The three-dimensional images were recorded on a Leica DMR XA2 motorized upright confocal microscope (software LCS 2). They were deconvolved with the commercial image restoration software Huygens 2.8 (Scientific Volume Imaging, Hilversum, The Netherlands) and visualized with the Imaris 6 software package (Bitplane AG, Zürich, Switzerland). Quantitative image analyses were performed by processing the three-dimensional multi-channel images with a dedicated image-analysis software that we have developed for our study. This software contains the following three-dimensional image-processing tools: denoising by Gaussian filtering, automatic threshold using the fluorescence background as baseline, a connected-component labeling and a function that evaluates the distance of each voxel to the closest detected border. All the multi-channel interaction measurements were collected in a spreadsheet for further statistical analysis. The software 'Volumetric Segmentation' was developed as a Java plugin for the public domain image-processing software, ImageJ 1.37 (National Institutes of Health, Bethesda, MD, USA); it is available online at: http://bigwww.epfl.ch/sage/soft/volumetricsegm/.

Immuno-electron microscopy

Eight weeks post-injection, rats destined to IEM analyses were deeply anesthetized by an overdose of pentobarbital and perfused transcardially first with 0.9% NaCl and then with ice-cold 4% PFA (Fluka-Sigma). Brains were rapidly removed and kept in 4% PFA overnight. Thirty μm-thick coronal sections from the SN were harvested on a sliding microtome (Leica SM2400; Leica) at a temperature of −20°C. Slices were then treated as described previously (102). The secondary antibody was an F(ab')2 fragment of goat anti-mouse from AURION Ultra Small Immunogold Reagents. Ultrastructural studies were performed on ultrathin sections (40 nm), stained with uranyl acetate and Reynold's lead citrate and viewed with a Philips CM-100 TEM electron microscope.

Statistical analyses

The Statistica program (StatSoft, France) was used for all calculations. One-way analysis of variance (103), followed by Scheffé's *post hoc* test, revealed a main group effect in all cases.

ACKNOWLEDGEMENTS

The authors thank Vivianne Padrun, Fabienne Pidoux, Christel Sadeghi, Anne Maillard, Philippe Colin and Jocelyne Bureau for excellent technical assistance. We are grateful to Jean-Charles Bensadoun for statistical analyses and to Cédric Raoul and Matthias Cacquevel for their valuable advice.

Conflict of Interest statement. None declared.

FUNDING

This work was funded by grants from the Swiss National Science Foundation and the Michael J. Fox Foundation.

REFERENCES

1. Fujiwara, H., Hasegawa, M., Dohmae, N., Kawashima, A., Masliah, E., Goldberg, M.S., Shen, J., Takio, K. and Iwatsubo, T. (2002) alpha-Synuclein is phosphorylated in synucleinopathy lesions. *Nat. Cell Biol.*, **4**, 160–164.
2. Mori, F., Tanji, K., Zhang, H., Kakita, A., Takahashi, H. and Wakabayashi, K. (2007) alpha-Synuclein pathology in the neostriatum in Parkinson's disease. *Acta Neuropathol.*, **115**, 453–459.
3. Nishie, M., Mori, F., Fujiwara, H., Hasegawa, M., Yoshimoto, M., Iwatsubo, T., Takahashi, H. and Wakabayashi, K. (2004) Accumulation of phosphorylated alpha-synuclein in the brain and peripheral ganglia of patients with multiple system atrophy. *Acta Neuropathol.*, **107**, 292–298.
4. Obi, K., Akiyama, H., Kondo, H., Shimomura, Y., Hasegawa, M., Iwatsubo, T., Mizuno, Y. and Mochizuki, H. (2008) Relationship of phosphorylated alpha-synuclein and tau accumulation to Abeta deposition in the cerebral cortex of dementia with Lewy bodies. *Exp. Neurol.*, **210**, 409–420.
5. Saito, Y., Kawashima, A., Ruberu, N.N., Fujiwara, H., Koyama, S., Sawabe, M., Arai, T., Nagura, H., Yamanouchi, H., Hasegawa, M. *et al.* (2003) Accumulation of phosphorylated alpha-synuclein in aging human brain. *J. Neuropathol. Exp. Neurol.*, **62**, 644–654.
6. Kruger, R., Kuhn, W., Muller, T., Woitalla, D., Graeber, M., Kosel, S., Przuntek, H., Epplen, J.T., Schols, L. and Riess, O. (1998) Ala30Pro mutation in the gene encoding alpha-synuclein in Parkinson's disease. *Nat. Genet.*, **18**, 106–108.
7. Lee, M.K., Stirling, W., Xu, Y., Xu, X., Qui, D., Mandir, A.S., Dawson, T.M., Copeland, N.G., Jenkins, N.A. and Price, D.L. (2002) Human alpha-synuclein-harboring familial Parkinson's disease-linked Ala-53→Thr mutation causes neurodegenerative disease with alpha-synuclein aggregation in transgenic mice. *Proc. Natl Acad. Sci. USA*, **99**, 8968–8973.
8. Polymeropoulos, M.H., Lavedan, C., Leroy, E., Ide, S.E., Dehejia, A., Dutra, A., Pike, B., Root, H., Rubenstein, J., Boyer, R. *et al.* (1997) Mutation in the alpha-synuclein gene identified in families with Parkinson's disease. *Science*, **276**, 2045–2047.
9. Spillantini, M.G., Schmidt, M.L., Lee, V.M., Trojanowski, J.Q., Jakes, R. and Goedert, M. (1997) Alpha-synuclein in Lewy bodies. *Nature*, **388**, 839–840.
10. Zarranz, J.J., Alegre, J., Gomez-Esteban, J.C., Lezcano, E., Ros, R., Ampuero, I., Vidal, L., Hoenicka, J., Rodriguez, O., Atares, B. *et al.* (2004) The new mutation, E46K, of alpha-synuclein causes Parkinson and Lewy body dementia. *Ann. Neurol.*, **55**, 164–173.
11. Duda, J.E., Giasson, B.I., Mabon, M.E., Miller, D.C., Golbe, L.I., Lee, V.M. and Trojanowski, J.Q. (2002) Concurrence of alpha-synuclein and tau brain pathology in the Contursi kindred. *Acta Neuropathol.*, **104**, 7–11.
12. Farrer, M., Kachergus, J., Forno, L., Lincoln, S., Wang, D.S., Hulihan, M., Maraganore, D., Gwinn-Hardy, K., Wszolek, Z., Dickson, D. *et al.* (2004) Comparison of kindreds with parkinsonism and alpha-synuclein genomic multiplications. *Ann. Neurol.*, **55**, 174–179.
13. Miller, D.W., Hague, S.M., Clarimon, J., Baptista, M., Gwinn-Hardy, K., Cookson, M.R. and Singleton, A.B. (2004) Alpha-synuclein in blood and brain from familial Parkinson disease with SNCA locus triplication. *Neurology*, **62**, 1835–1838.

14. Nishioka, K., Hayashi, S., Farrer, M.J., Singleton, A.B., Yoshino, H., Imai, H., Kitami, T., Sato, K., Kuroda, R., Tomiyama, H. *et al.* (2006) Clinical heterogeneity of alpha-synuclein gene duplication in Parkinson's disease. *Ann. Neurol.*, **59**, 298–309.
15. Singleton, A.B., Farrer, M., Johnson, J., Singleton, A., Hague, S., Kachergus, J., Hulihan, M., Peuralinna, T., Dutra, A., Nussbaum, R. *et al.* (2003) alpha-Synuclein locus triplication causes Parkinson's disease. *Science*, **302**, 841.
16. Anderson, J.P., Walker, D.E., Goldstein, J.M., de Laat, R., Banducci, K., Caccavello, R.J., Barbour, R., Huang, J., Kling, K., Lee, M. *et al.* (2006) Phosphorylation of Ser-129 is the dominant pathological modification of alpha-synuclein in familial and sporadic Lewy body disease. *J. Biol. Chem.*, **281**, 29739–29752.
17. Hasegawa, M., Fujiwara, H., Nonaka, T., Wakabayashi, K., Takahashi, H., Lee, V.M., Trojanowski, J.Q., Mann, D. and Iwatsubo, T. (2002) Phosphorylated alpha-synuclein is ubiquitinated in alpha-synucleinopathy lesions. *J. Biol. Chem.*, **277**, 49071–49076.
18. Neumann, M., Kahle, P.J., Giasson, B.I., Ozmen, L., Borroni, E., Spooren, W., Muller, V., Odoy, S., Fujiwara, H., Hasegawa, M. *et al.* (2002) Misfolded proteinase K-resistant hyperphosphorylated alpha-synuclein in aged transgenic mice with locomotor deterioration and in human alpha-synucleinopathies. *J. Clin. Invest.*, **110**, 1429–1439.
19. Bodner, R.A., Housman, D.E. and Kazantsev, A.G. (2006) New directions for neurodegenerative disease therapy: using chemical compounds to boost the formation of mutant protein inclusions. *Cell Cycle*, **5**, 1477–1480.
20. Bucciantini, M., Calloni, G., Chiti, F., Formigli, L., Nosi, D., Dobson, C.M. and Stefani, M. (2004) Prefibrillar amyloid protein aggregates share common features of cytotoxicity. *J. Biol. Chem.*, **279**, 31374–31382.
21. Conway, K.A., Harper, J.D. and Lansbury, P.T. Jr (2000) Fibrils formed *in vitro* from alpha-synuclein and two mutant forms linked to Parkinson's disease are typical amyloid. *Biochemistry*, **39**, 2552–2563.
22. El-Agnaf, O.M., Salem, S.A., Paleologou, K.E., Curran, M.D., Gibson, M.J., Court, J.A., Schlossmacher, M.G. and Allsop, D. (2006) Detection of oligomeric forms of alpha-synuclein protein in human plasma as a potential biomarker for Parkinson's disease. *FASEB J.*, **20**, 419–425.
23. Goldberg, M.S. and Lansbury, P.T. Jr (2000) Is there a cause-and-effect relationship between alpha-synuclein fibrillization and Parkinson's disease? *Nat. Cell Biol.*, **2**, E115–E119.
24. Kayed, R., Head, E., Thompson, J.L., McIntire, T.M., Milton, S.C., Cotman, C.W. and Glabe, C.G. (2003) Common structure of soluble amyloid oligomers implies common mechanism of pathogenesis. *Science*, **300**, 486–489.
25. Kayed, R., Sokolov, Y., Edmonds, B., McIntire, T.M., Milton, S.C., Hall, J.E. and Glabe, C.G. (2004) Permeabilization of lipid bilayers is a common conformation-dependent activity of soluble amyloid oligomers in protein misfolding diseases. *J. Biol. Chem.*, **279**, 46363–46366.
26. Park, J.Y. and Lansbury, P.T. Jr (2003) Beta-synuclein inhibits formation of alpha-synuclein protofibrils: a possible therapeutic strategy against Parkinson's disease. *Biochemistry*, **42**, 3696–3700.
27. Leger, J., Kempf, M., Lee, G. and Brandt, R. (1997) Conversion of serine to aspartate imitates phosphorylation-induced changes in the structure and function of microtubule-associated protein tau. *J. Biol. Chem.*, **272**, 8441–8446.
28. Corbit, K.C., Trakul, N., Eves, E.M., Diaz, B., Marshall, M. and Rosner, M.R. (2003) Activation of Raf-1 signaling by protein kinase C through a mechanism involving Raf kinase inhibitory protein. *J. Biol. Chem.*, **278**, 13061–13068.
29. Richards, J.P., Bachinger, H.P., Goodman, R.H. and Brennan, R.G. (1996) Analysis of the structural properties of cAMP-responsive element-binding protein (CREB) and phosphorylated CREB. *J. Biol. Chem.*, **271**, 13716–13723.
30. Chen, L. and Feany, M.B. (2005) Alpha-synuclein phosphorylation controls neurotoxicity and inclusion formation in a *Drosophila* model of Parkinson disease. *Nat. Neurosci.*, **8**, 657–663.
31. Gorbatyuk, O.S., Li, S., Sullivan, L.F., Chen, W., Kondrikova, G., Manfredsson, F.P., Mandel, R.J. and Muzyczka, N. (2008) The phosphorylation state of Ser-129 in human alpha-synuclein determines neurodegeneration in a rat model of Parkinson disease. *Proc. Natl Acad. Sci. USA*, **105**, 763–768.
32. Goedert, M. (2001) Alpha-synuclein and neurodegenerative diseases. *Nat. Rev. Neurosci.*, **2**, 492–501.
33. Hamilton, B.A. (2004) alpha-Synuclein A53T substitution associated with Parkinson disease also marks the divergence of Old World and New World primates. *Genomics*, **83**, 739–742.
34. LeVine, H. III (1999) Quantification of beta-sheet amyloid fibril structures with thioflavin T. *Methods Enzymol.*, **309**, 274–284.
35. Eslamboli, A., Romero-Ramos, M., Burger, C., Bjorklund, T., Muzyczka, N., Mandel, R.J., Baker, H., Ridley, R.M. and Kirik, D. (2007) Long-term consequences of human alpha-synuclein overexpression in the primate ventral midbrain. *Brain*, **130**, 799–815.
36. Goers, J., Manning-Bog, A.B., McCormack, A.L., Millett, I.S., Doniach, S., Di Monte, D.A., Uversky, V.N. and Fink, A.L. (2003) Nuclear localization of alpha-synuclein and its interaction with histones. *Biochemistry.*, **42**, 8465–8471.
37. Wakamatsu, M., Ishii, A., Ukai, Y., Sakagami, J., Iwata, S., Ono, M., Matsumoto, K., Nakamura, A., Tada, N., Kobayashi, K. *et al.* (2007) Accumulation of phosphorylated alpha-synuclein in dopaminergic neurons of transgenic mice that express human alpha-synuclein. *J. Neurosci. Res.*, **85**, 1819–1825.
38. Yamada, M., Iwatsubo, T., Mizuno, Y. and Mochizuki, H. (2004) Overexpression of alpha-synuclein in rat substantia nigra results in loss of dopaminergic neurons, phosphorylation of alpha-synuclein and activation of caspase-9: resemblance to pathogenetic changes in Parkinson's disease. *J. Neurochem.*, **91**, 451–461.
39. Arawaka, S., Wada, M., Goto, S., Karube, H., Sakamoto, M., Ren, C.H., Koyama, S., Nagasawa, H., Kimura, H., Kawanami, T. *et al.* (2006) The role of G-protein-coupled receptor kinase 5 in pathogenesis of sporadic Parkinson's disease. *J. Neurosci.*, **26**, 9227–9238.
40. Lee, G., Tanaka, M., Park, K., Lee, S.S., Kim, Y.M., Junn, E., Lee, S.H. and Mouradian, M.M. (2004) Casein kinase II-mediated phosphorylation regulates alpha-synuclein/synphilin-1 interaction and inclusion body formation. *J. Biol. Chem.*, **279**, 6834–6839.
41. Narayanan, V. and Scarlata, S. (2001) Membrane binding and self-association of alpha-synucleins. *Biochemistry*, **40**, 9927–9934.
42. Pronin, A.N., Morris, A.J., Surguchov, A. and Benovic, J.L. (2000) Synucleins are a novel class of substrates for G protein-coupled receptor kinases. *J. Biol. Chem.*, **275**, 26515–26522.
43. Smith, W.W., Margolis, R.L., Li, X., Troncoso, J.C., Lee, M.K., Dawson, V.L., Dawson, T.M., Iwatsubo, T. and Ross, C.A. (2005) Alpha-synuclein phosphorylation enhances eosinophilic cytoplasmic inclusion formation in SH-SY5Y cells. *J. Neurosci.*, **25**, 5544–5552.
44. Chen, Z., Hagler, J., Palombella, V.J., Melandri, F., Scherer, D., Ballard, D. and Maniatis, T. (1995) Signal-induced site-specific phosphorylation targets I kappa B alpha to the ubiquitin–proteasome pathway. *Genes Dev.*, **9**, 1586–1597.
45. Marienfeld, R., Berberich-Siebelt, F., Berberich, I., Denk, A., Serfling, E. and Neumann, M. (2001) Signal-specific and phosphorylation-dependent RelB degradation: a potential mechanism of NF-kappaB control. *Oncogene*, **20**, 8142–8147.
46. Rivedal, E. and Leithe, E. (2005) Connexin43 synthesis, phosphorylation, and degradation in regulation of transient inhibition of gap junction intercellular communication by the phorbol ester TPA in rat liver epithelial cells. *Exp. Cell Res.*, **302**, 143–152.
47. Kirik, D., Rosenblad, C., Burger, C., Lundberg, C., Johansen, T.E., Muzyczka, N., Mandel, R.J. and Bjorklund, A. (2002) Parkinson-like neurodegeneration induced by targeted overexpression of alpha-synuclein in the nigrostriatal system. *J. Neurosci.*, **22**, 2780–2791.
48. Klein, R.L., King, M.A., Hamby, M.E. and Meyer, E.M. (2002) Dopaminergic cell loss induced by human A30P alpha-synuclein gene transfer to the rat substantia nigra. *Hum. Gene Ther.*, **13**, 605–612.
49. Maingay, M., Romero-Ramos, M. and Kirik, D. (2005) Viral vector mediated overexpression of human alpha-synuclein in the nigrostriatal dopaminergic neurons: a new model for Parkinson's disease. *CNS Spectr.*, **10**, 235–244.
50. Bandhyopadhyay, U. and Cuervo, A.M. (2007) Chaperone-mediated autophagy in aging and neurodegeneration: lessons from alpha-synuclein. *Exp. Gerontol.*, **42**, 120–128.
51. Cuervo, A.M., Stefanis, L., Fredenburg, R., Lansbury, P.T. and Sulzer, D. (2004) Impaired degradation of mutant alpha-synuclein by chaperone-mediated autophagy. *Science*, **305**, 1292–1295.
52. Lee, H.J., Khoshaghideh, F., Patel, S. and Lee, S.J. (2004) Clearance of alpha-synuclein oligomeric intermediates via the lysosomal degradation pathway. *J. Neurosci.*, **24**, 1888–1896.

53. Webb, J.L., Ravikumar, B., Atkins, J., Skepper, J.N. and Rubinsztein, D.C. (2003) Alpha-synuclein is degraded by both autophagy and the proteasome. *J. Biol. Chem.*, **278**, 25009–25013.
54. Di Fonzo, A., Chien, H.F., Socal, M., Giraudo, S., Tassorelli, C., Iliceto, G., Fabbrini, G., Marconi, R., Fincati, E., Abbruzzese, G. *et al.* (2007) ATP13A2 missense mutations in juvenile parkinsonism and young onset Parkinson disease. *Neurology*, **68**, 1557–1562.
55. Pan, T., Kondo, S., Le, W. and Jankovic, J. (2008) The role of autophagy–lysosome pathway in neurodegeneration associated with Parkinson's disease. *Brain*, **131**, 1969–1978.
56. Ramirez, A., Heimbach, A., Grundemann, J., Stiller, B., Hampshire, D., Cid, L.P., Goebel, I., Mubaidin, A.F., Wriekat, A.L., Roeper, J. *et al.* (2006) Hereditary parkinsonism with dementia is caused by mutations in ATP13A2, encoding a lysosomal type 5 P-type ATPase. *Nat. Genet.*, **38**, 1184–1191.
57. Smith, W.W., Jiang, H., Pei, Z., Tanaka, Y., Morita, H., Sawa, A., Dawson, V.L., Dawson, T.M. and Ross, C.A. (2005) Endoplasmic reticulum stress and mitochondrial cell death pathways mediate A53T mutant alpha-synuclein-induced toxicity. *Hum. Mol. Genet.*, **14**, 3801–3811.
58. Tanaka, Y., Engelender, S., Igarashi, S., Rao, R.K., Wanner, T., Tanzi, R.E., Sawa, A., Dawson, V.L., Dawson, T.M. and Ross, C.A. (2001) Inducible expression of mutant alpha-synuclein decreases proteasome activity and increases sensitivity to mitochondria-dependent apoptosis. *Hum. Mol. Genet.*, **10**, 919–926.
59. Wang, H.Q. and Takahashi, R. (2007) Expanding insights on the involvement of endoplasmic reticulum stress in Parkinson's disease. *Antioxid. Redox Signal.*, **9**, 553–561.
60. Bence, N.F., Sampat, R.M. and Kopito, R.R. (2001) Impairment of the ubiquitin–proteasome system by protein aggregation. *Science*, **292**, 1552–1555.
61. Gonatas, N.K., Gonatas, J.O. and Stieber, A. (1998) The involvement of the Golgi apparatus in the pathogenesis of amyotrophic lateral sclerosis, Alzheimer's disease, and ricin intoxication. *Histochem. Cell Biol.*, **109**, 591–600.
62. Lindholm, D., Wootz, H. and Korhonen, L. (2006) ER stress and neurodegenerative diseases. *Cell Death Differ.*, **13**, 385–392.
63. Sakurai, A., Okamoto, K., Fujita, Y., Nakazato, Y., Wakabayashi, K., Takahashi, H. and Gonatas, N.K. (2000) Fragmentation of the Golgi apparatus of the ballooned neurons in patients with corticobasal degeneration and Creutzfeldt–Jakob disease. *Acta Neuropathol.*, **100**, 270–274.
64. Sakurai, A., Okamoto, K., Yaguchi, M., Fujita, Y., Mizuno, Y., Nakazato, Y. and Gonatas, N.K. (2002) Pathology of the inferior olivary nucleus in patients with multiple system atrophy. *Acta Neuropathol.*, **103**, 550–554.
65. Cooper, A.A., Gitler, A.D., Cashikar, A., Haynes, C.M., Hill, K.J., Bhullar, B., Liu, K., Xu, K., Strathearn, K.E., Liu, F. *et al.* (2006) Alpha-synuclein blocks ER-Golgi traffic and Rab1 rescues neuron loss in Parkinson's models. *Science*, **313**, 324–328.
66. Hoozemans, J.J., van Haastert, E.S., Eikelenboom, P., de Vos, R.A., Rozemuller, J.M. and Scheper, W. (2007) Activation of the unfolded protein response in Parkinson's disease. *Biochem. Biophys. Res. Commun.*, **354**, 707–711.
67. Gosavi, N., Lee, H.J., Lee, J.S., Patel, S. and Lee, S.J. (2002) Golgi fragmentation occurs in the cells with prefibrillar alpha-synuclein aggregates and precedes the formation of fibrillar inclusion. *J. Biol. Chem.*, **277**, 48984–48992.
68. Lee, H.J., Khoshaghideh, F., Lee, S. and Lee, S.J. (2006) Impairment of microtubule-dependent trafficking by overexpression of alpha-synuclein. *Eur. J. Neurosci.*, **24**, 3153–3162.
69. Chiu, R., Novikov, L., Mukherjee, S. and Shields, D. (2002) A caspase cleavage fragment of p115 induces fragmentation of the Golgi apparatus and apoptosis. *J. Cell Biol.*, **159**, 637–648.
70. Lane, J.D., Lucocq, J., Pryde, J., Barr, F.A., Woodman, P.G., Allan, V.J. and Lowe, M. (2002) Caspase-mediated cleavage of the stacking protein GRASP65 is required for Golgi fragmentation during apoptosis. *J. Cell Biol.*, **156**, 495–509.
71. Fujita, Y., Ohama, E., Takatama, M., Al-Sarraj, S. and Okamoto, K. (2006) Fragmentation of Golgi apparatus of nigral neurons with alpha-synuclein-positive inclusions in patients with Parkinson's disease. *Acta Neuropathol.*, **112**, 261–265.
72. Mattson, M.P. (2006) Neuronal life-and-death signaling, apoptosis, and neurodegenerative disorders. *Antioxid. Redox Signal.*, **8**, 1997–2006.
73. Nakamura, K., Nemani, V.M., Wallender, E.K., Kaehlcke, K., Ott, M. and Edwards, R.H. (2008) Optical reporters for the conformation of {alpha}-synuclein reveal a specific interaction with mitochondria. *J. Neurosci.*, **28**, 12305–12317.
74. Parihar, M.S., Parihar, A., Fujita, M., Hashimoto, M. and Ghafourifar, P. (2008) Mitochondrial association of alpha-synuclein causes oxidative stress. *Cell Mol. Life Sci.*, **65**, 1272–1284.
75. Shavali, S., Brown-Borg, H.M., Ebadi, M. and Porter, J. (2008) Mitochondrial localization of alpha-synuclein protein in alpha-synuclein overexpressing cells. *Neurosci. Lett.*, **439**, 125–128.
76. Devi, L., Raghavendran, V., Prabhu, B.M., Avadhani, N.G. and Anandatheerthavarada, H.K. (2008) Mitochondrial import and accumulation of alpha-synuclein impair complex I in human dopaminergic neuronal cultures and Parkinson disease brain. *J. Biol. Chem.*, **283**, 9089–9100.
77. Hashimoto, M., Rockenstein, E., Crews, L. and Masliah, E. (2003) Role of protein aggregation in mitochondrial dysfunction and neurodegeneration in Alzheimer's and Parkinson's diseases. *Neuromolecular Med.*, **4**, 21–36.
78. Hsu, L.J., Sagara, Y., Arroyo, A., Rockenstein, E., Sisk, A., Mallory, M., Wong, J., Takenouchi, T., Hashimoto, M. and Masliah, E. (2000) alpha-synuclein promotes mitochondrial deficit and oxidative stress. *Am. J. Pathol.*, **157**, 401–410.
79. Martin, L.J., Pan, Y., Price, A.C., Sterling, W., Copeland, N.G., Jenkins, N.A., Price, D.L. and Lee, M.K. (2006) Parkinson's disease alpha-synuclein transgenic mice develop neuronal mitochondrial degeneration and cell death. *J. Neurosci.*, **26**, 41–50.
80. Stichel, C.C., Zhu, X.R., Bader, V., Linnartz, B., Schmidt, S. and Lubbert, H. (2007) Mono- and double-mutant mouse models of Parkinson's disease display severe mitochondrial damage. *Hum. Mol. Genet.*, **16**, 3377–3393.
81. Beal, M.F. (2004) Mitochondrial dysfunction and oxidative damage in Alzheimer's and Parkinson's diseases and coenzyme Q10 as a potential treatment. *J. Bioenerg. Biomembr.*, **36**, 381–386.
82. Mizuno, Y., Ikebe, S., Hattori, N., Nakagawa-Hattori, Y., Mochizuki, H., Tanaka, M. and Ozawa, T. (1995) Role of mitochondria in the etiology and pathogenesis of Parkinson's disease. *Biochim. Biophys. Acta.*, **1271**, 265–274.
83. Parker, W.D. Jr, Parks, J.K. and Swerdlow, R.H. (2008) Complex I deficiency in Parkinson's disease frontal cortex. *Brain Res.*, **1189**, 215–218.
84. Schapira, A.H. (2001) Causes of neuronal death in Parkinson's disease. *Adv. Neurol.*, **86**, 155–162.
85. Hartmann, A., Hunot, S., Michel, P.P., Muriel, M.P., Vyas, S., Faucheux, B.A., Mouatt-Prigent, A., Turmel, H., Srinivasan, A., Ruberg, M. *et al.* (2000) Caspase-3: a vulnerability factor and final effector in apoptotic death of dopaminergic neurons in Parkinson's disease. *Proc. Natl Acad. Sci. USA*, **97**, 2875–2880.
86. Tatton, N.A. (2000) Increased caspase 3 and Bax immunoreactivity accompany nuclear GAPDH translocation and neuronal apoptosis in Parkinson's disease. *Exp. Neurol.*, **166**, 29–43.
87. Tatton, W.G., Chalmers-Redman, R., Brown, D. and Tatton, N. (2003) Apoptosis in Parkinson's disease: signals for neuronal degradation. *Ann. Neurol.*, **53** (Suppl 3), S61–S70. discussion S70-62.
88. Kerr, J.F., Wyllie, A.H. and Currie, A.R. (1972) Apoptosis: a basic biological phenomenon with wide-ranging implications in tissue kinetics. *Br. J. Cancer*, **26**, 239–257.
89. Duce, J.A., Smith, D.P., Blake, R.E., Crouch, P.J., Li, Q.X., Masters, C.L. and Trounce, I.A. (2006) Linker histone H1 binds to disease associated amyloid-like fibrils. *J. Mol. Biol.*, **361**, 493–505.
90. Kontopoulos, E., Parvin, J.D. and Feany, M.B. (2006) Alpha-synuclein acts in the nucleus to inhibit histone acetylation and promote neurotoxicity. *Hum. Mol. Genet.*, **15**, 3012–3023.
91. Gomez-Isla, T., Irizarry, M.C., Mariash, A., Cheung, B., Soto, O., Schrump, S., Sondel, J., Kotilinek, L., Day, J., Schwarzschild, M.A. *et al.* (2003) Motor dysfunction and gliosis with preserved dopaminergic markers in human alpha-synuclein A30P transgenic mice. *Neurobiol. Aging.*, **24**, 245–258.
92. Kahle, P.J., Neumann, M., Ozmen, L., Muller, V., Jacobsen, H., Schindzielorz, A., Okochi, M., Leimer, U., van Der Putten, H., Probst, A. *et al.* (2000) Subcellular localization of wild-type and Parkinson's

disease-associated mutant alpha-synuclein in human and transgenic mouse brain. *J. Neurosci.*, **20**, 6365–6373.
93. Richfield, E.K., Thiruchelvam, M.J., Cory-Slechta, D.A., Wuertzer, C., Gainetdinov, R.R., Caron, M.G., Di Monte, D.A. and Federoff, H.J. (2002) Behavioral and neurochemical effects of wild-type and mutated human alpha-synuclein in transgenic mice. *Exp. Neurol.*, **175**, 35–48.
94. Rockenstein, E., Mallory, M., Hashimoto, M., Song, D., Shults, C.W., Lang, I. and Masliah, E. (2002) Differential neuropathological alterations in transgenic mice expressing alpha-synuclein from the platelet-derived growth factor and Thy-1 promoters. *J. Neurosci. Res.*, **68**, 568–578.
95. Bradbury, J. (2003) Alpha-synuclein gene triplication discovered in Parkinson's disease. *Lancet Neurol.*, **2**, 715.
96. Ikeuchi, T., Kakita, A., Shiga, A., Kasuga, K., Kaneko, H., Tan, C.F., Idezuka, J., Wakabayashi, K., Onodera, O., Iwatsubo, T. *et al.* (2008) Patients homozygous and heterozygous for SNCA duplication in a family with parkinsonism and dementia. *Arch. Neurol.*, **65**, 514–519.
97. Eriksen, J.L., Przedborski, S. and Petrucelli, L. (2005) Gene dosage and pathogenesis of Parkinson's disease. *Trends Mol. Med.*, **11**, 91–96.
98. Kim, E.J., Sung, J.Y., Lee, H.J., Rhim, H., Hasegawa, M., Iwatsubo, T., Min do, S., Kim, J., Paik, S.R. and Chung, K.C. (2006) Dyrk1A phosphorylates alpha-synuclein and enhances intracellular inclusion formation. *J. Biol. Chem.*, **281**, 33250–33257.
99. Okochi, M., Walter, J., Koyama, A., Nakajo, S., Baba, M., Iwatsubo, T., Meijer, L., Kahle, P.J. and Haass, C. (2000) Constitutive phosphorylation of the Parkinson's disease associated alpha-synuclein. *J. Biol. Chem.*, **275**, 390–397.
100. Paleologou, K.E., Schmid, A.W., Rospigliosi, C.C., Kim, H.Y., Lamberto, G.R., Fredenburg, R.A., Lansbury, P.T. Jr, Fernandez, C.O., Eliezer, D., Zweckstetter, M. *et al.* (2008) Phosphorylation at S129, but not the phosphomimics S129E/D inhibits the fibrilization of alpha-synuclein. *J. Biol. Chem*., **283**, 16895–16905.
101. Grimm, D., Kay, M.A. and Kleinschmidt, J.A. (2003) Helper virus-free, optically controllable, and two-plasmid-based production of adeno-associated virus vectors of serotypes 1 to 6. *Mol. Ther.*, **7**, 839–850.
102. Yi, H., Leunissen, J., Shi, G., Gutekunst, C. and Hersch, S. (2001) A novel procedure for pre-embedding double immunogold-silver labeling at the ultrastructural level. *J. Histochem. Cytochem.*, **49**, 279–284.
103. Stefanova, N., Klimaschewski, L., Poewe, W., Wenning, G.K. and Reindl, M. (2001) Glial cell death induced by overexpression of alpha-synuclein. *J. Neurosci. Res.*, **65**, 432–438.